Plxdc family members are novel receptors for the rhesus monkey rhadinovirus (RRV)

Running Head: Plxdcs are receptors for the Rhesus Monkey Rhadinovirus

Anna K. Großkopf[a], Sarah Schlagowski[a], Thomas Fricke[a], Armin Ensser[b], Ronald C. Desrosiers[c], Alexander S. Hahn[a]

[a] German Primate Center - Leibniz Institute for Primate Research, Göttingen, Germany

[b] Universitätsklinikum Erlangen, Institute for Clinical and Molecular Virology, Erlangen, Germany

[c] Miller School of Medicine, University of Miami, Miami, United States

#Address correspondence to Alexander S. Hahn, ahahn@dpz.eu

ABSTRACT

The rhesus monkey rhadinovirus (RRV), a γ2-herpesvirus of rhesus macaques, shares many biological features with the human pathogenic Kaposi's sarcoma-associated herpesvirus (KSHV). Both viruses, as well as the more distantly related Epstein-Barr virus, engage cellular receptors from the Eph family of receptor tyrosine kinases (Ephs). However, the importance of the Eph interaction for RRV entry varies between cell types suggesting the existence of Eph-independent entry pathways. We therefore aimed to identify additional cellular receptors for RRV by affinity enrichment and mass spectrometry. We identified an additional receptor family, the Plexin domain containing proteins 1 and 2 (Plxdc1/2) that bind the RRV gH/gL glycoprotein complex. Preincubation of RRV with soluble Plxdc2 decoy receptor reduced infection by approx. 60%, while overexpression of Plxdc1 and 2 dramatically enhanced RRV

susceptibility of otherwise marginally permissive Raji cells. While the Plxdc2 interaction is conserved between two RRV strains, 26-95 and 17577, Plxdc1 specifically interacts with RRV 26-95 gH. The Plxdc interaction is mediated by a short motif at the N-terminus of RRV gH that is partially conserved between isolate 26-95 and isolate 17577, but absent in KSHV gH. Mutation of this motif abrogated the interaction with Plxdc1/2 in *in vitro* assays and reduced RRV infection in a cell-type specific manner. Taken together, our findings characterize Plxdc1/2 as novel interaction partners and entry receptors for RRV and support the concept of the N-terminal domain of the gammaherpesviral gH/gL complex as a multifunctional receptor-binding domain. Further, Plxdc1/2 usage defines an important biological difference between KSHV and RRV.

AUTHORS SUMMARY

KSHV is the causative agent of a group of malignancies which account for a substantial disease burden in particular in sub-Saharan Africa. RRV, a related virus of rhesus macaques, has shown promise as model system for KSHV and for the development of immunization strategies. To exploit the full potential of the RRV animal model system, detailed knowledge of commonalities and differences between KSHV and RRV is key. Here, we describe the Plexin domain containing proteins 1 and 2 as a novel receptor family which mediates entry of RRV, but not of KSHV. Infection experiments using RRV mutants deleted of the Plxdc interaction motif suggest a cell type-specific contribution of Plxdc receptors to RRV infection. As information on Plxdc1/2 and its biological function is still sparse, analysis of the RRV–Plxdc interaction will help to characterize the physiological and pathophysiological role of this receptor family.

INTRODUCTION

The rhesus monkey rhadinovirus (RRV), a member of the genus γ2-herpesvirus or rhadinovirus, is closely related to the only human pathogenic member of this genus, the Kaposi's sarcoma-associated

48 herpesvirus (KSHV) (1, 2). Due to the high similarity in both genome organization and biology RRV is
49 considered as an animal model virus for KSHV (3) and has been used as such in *in vitro* and *in vivo*
50 studies. Two major RRV sequence groups have been identified (4), and each is represented by a cloned
51 isolate, RRV 26-95 (5) and RRV 17577 (6). Analogous to KSHV infection, primary RRV infection is
52 asymptomatic in healthy hosts and leads to life-long persistence, most likely in the B cell compartment
53 (7). KSHV is associated with a solid tumor of endothelial origin, Kaposi's sarcoma (KS), and two B cell
54 malignancies, primary effusion lymphoma (PEL) and the plasmablastic variant of multicentric
55 Castleman's disease (MCD), most prominently in the context of human immunodeficiency virus (HIV)
56 infection and in immunocompromised individuals. Similarly, simian immunodeficiency virus (SIV)-
57 positive rhesus macaques developed B cell lymphomas upon experimental infection with RRV strain
58 17577 (8, 9) and several studies correlated RRV infection with lymphomagenesis in SIV/SHIV-infected
59 animals (10, 11). While RRV is not consistently associated with solid malignancies, RRV has been
60 identified in retroperitoneal fibromatosis tissue (9, 12), similar to retroperitoneal fibromatosis
61 herpesvirus (RFHV)(11), and was recently isolated from hemangioma tissue (13). Another shared
62 characteristic of KSHV and RRV is the receptor usage on a range of cell types. Both viruses engage
63 members of the Eph family of receptor tyrosine kinases (Ephs) through their glycoprotein (g)H/gL
64 complex to facilitate entry into target cells. While KSHV preferentially interacts with A-type Ephs –
65 specifically EphA2 as the high affinity receptor (14, 15) – RRV can utilize both A- and B-type Ephs (15)
66 for entry. These interactions have been characterized on different adherent cells types (6–9) and we
67 could recently show that both viruses can utilize EphA7 as receptor on BJAB cells (20), a model B
68 lymphocyte line. While for KSHV, in addition to Eph family receptors, several membrane proteins have
69 been proposed as cellular receptors for different viral glycoproteins mediating either attachment or
70 entry on a range of target cells (reviewed in (21)) the receptor usage of RRV is comparatively less well
71 characterized. Nevertheless, studies using receptor knock-down or knockout (14, 22), receptor- and
72 ligand-mediated blocking (15, 23), and Eph de-targeted virus mutants (23, 24) showed that both
73 viruses and in particular RRV can infect various cells partially or completely independently of the Eph-

74 interaction, which suggests that RRV engages at least one additional entry receptor that can
75 functionally substitute for the Eph-interaction. This notion is also supported by a recent *in vivo* study
76 that demonstrated that an RRV mutant deleted of gL and therefore unable to interact with Eph
77 receptors still establishes persistent infection in RRV-naïve rhesus macaques upon intravenous
78 inoculation (24). We therefore aimed to identify additional rhadinovirus receptors that bind the gH/gL
79 complex or gH and identified Plexin domain containing protein 2 (Plxdc2) as novel interaction partner
80 of the gH/gL complex of RRV, but not KSHV. The closest homolog to Plxdc2, Plxdc1 was initially
81 identified as overexpressed in blood vessels of solid human tumors (25), resulting in the original
82 terminology tumor endothelial marker 7 (TEM7, Plxdc1) and tumor endothelial marker 7 related
83 (TEM7R, Plxdc2) (26). In general, the physiological functions of Plxdc1/2 are not well understood.
84 Suggestive of a role in development, Plxdc2 has been described as mitogen for neural progenitor cells
85 (27) and expression of both Plxdc1 and Plxdc2 in the developing nervous system has been
86 demonstrated (28, 29). Cortactin, nidogen and the pigment epithelium derived factor (PEDF) have
87 been described as interactors for Plxdc1 and Plxdc2 (30–32). However, the physiological relevance of
88 these interactions is not fully understood. In this study we characterize the interaction of Plxdc1/2 with
89 the gH/gL glycoprotein complex of RRV and establish Plxdcs as novel cellular RRV entry receptors.

90

91 **RESULTS**

92 To identify potential cellular receptors for RRV glycoprotein H, we performed
93 immunoprecipitation using soluble RRV 26-95 gH, consisting of the extracellular part fused to the Fc
94 part of human IgG (RRV gH-FcStrep) as bait and 293T whole cell lysate as prey (Fig 1A). Bands present
95 in the precipitation from 293T whole cell lysate, but not in control precipitation without 293T lysate
96 were excised and analyzed by LC-MS/MS. The most abundant cell surface protein, identified in four of
97 the five analyzed regions, was Plxdc2 or TEM7R, a cellular transmembrane protein. As described above,
98 Plxdc1 or TEM7 is the only homolog of Plxdc2 in humans and rhesus macaques, and was therefore

99 included in subsequent analyses. Human and rhesus Plxdc1 (ref |NM_020405.5|; ref
100 |XM_028836436.1|) and Plxdc2 (ref |NM_032812.9|; ref |XM_028826043.1|) are 96.80% and 97.92%
101 identical on the amino sequence level.

102 Co-immunoprecipitation of V5-tagged expression constructs of gH from KSHV and from the
103 two RRV isolates 26-95 and 17577, in the presence or absence of the corresponding Flag-tagged gL
104 proteins with myc-tagged human Plxdc1 or Plxdc2 (hPlxdc1-myc/ hPlxdc2-myc) from transfected 293T
105 cells confirmed the interaction of both RRV gH/gL complexes with Plxdc2 (Fig 1B). Neither KSHV gH/gL
106 nor RRV 17577 gH/gL interacted detectably with Plxdc1-myc, while RRV 26-95 prominently bound both
107 Plxdc1 and Plxdc2 in the presence and absence of gL. Measurement of the binding of purified Plxdc1
108 and Plxdc2 ectodomain to immobilized RRV 26-95 gH-FcStrep/gL by enzyme-linked immunosorbent
109 assay (Fig 1C, D) showed a half-maximal binding concentration of 22.2nM for Plxdc1 and 5.2nM for
110 Plxdc2 as calculated for one site specific binding without pre-defined Hill slope.

111 To evaluate the effect of Plxdc-binding to RRV gH on the interaction with EphB3, the high-
112 affinity Eph family receptor for RRV gH/gL (15), we used soluble human Plxdc1 or Plxdc2, consisting of
113 the extracellular part of Plxdc1 or Plxdc2 fused to the Fc part of human IgG followed by a TwinStrep
114 tag (hPlxdc1-FcStrep/ hPlxdc2-FcStrep) in immunoprecipitation experiments. Co-immunoprecipitation
115 of hPlxdc1-FcStrep/ hPlxdc2-FcStrep with the gH-V5/gL-Flag complexes of RRV isolates 26-95 and
116 17577 in the presence or absence of myc-tagged EphB3 from transfected 293T cells demonstrated the
117 existence of a quaternary complex, indicating the ability of RRV gH/gL to interact with members of
118 both receptor families simultaneously (Fig 1E).

119 While interaction of purified proteins and in transfected cell lysates is strongly suggestive of a
120 functional interaction, the biologically relevant interaction for the entry process would occur with
121 virion gH/gL. To evaluate the functionality of the gH/gL-Plxdc interaction on virus particles both for
122 wildtype RRV and an Eph-binding-negative RRV mutant, we utilized RRV-YFP, an RRV 26-95 strain
123 engineered for constitutive YFP expression upon infection, and RRV-YFP gH-AELAAN, an Eph-binding-

124 negative RRV-YFP mutant that we had previously described (Fig 2A) (23). To analyze the impact of
125 competition with soluble Plxdc decoy receptor, RRV-YFP wt and RRV-YFP gH-AELAAN preparations
126 were incubated with a concentration series of soluble hPlxdc2-FcStrep or an FcStrep control prior to
127 infection of HaCaT cells (Fig 2B). According to RNA-Seq data of 36 cell lines (Courtesy of Human Protein
128 Atlas, www.proteinatlas.org, (33)), HaCaT cells exhibit the highest cell-line specific expression of Plxdc2
129 among the analyzed non-cancer cell lines and were therefore chosen for further analyses. Soluble
130 Plxdc2-FcStrep inhibited RRV-YFP wt infection up to approx. 60% in a dose dependent manner when
131 compared to FcStrep alone. Likewise, preincubation of RRV-YFP gH-AELAAN with hPlxdc2-FcStrep
132 reduced infection by approx. 65%. RRV-YFP wt and RRV-YFP gH-AELAAN infection was normalized to
133 approx. MOI 0.2. Inhibition of the gH/gL-Eph interaction, which served as control, lead to an approx.
134 50% reduction of RRV-YFP wt infection at a concentration of 10nM hEphB3-Fc while 100nM of soluble
135 hPlxdc2-FcStrep exhibited a similar blocking efficiency. Preincubation with both hEphB3-Fc and
136 hPlxdc2-FcStrep further reduced RRV-YFP wt infection on HaCaT cells, when compared to
137 preincubation with either hEphB3-Fc or hPlxdc2-FcStrep alone (Fig 2C). While preincubation with
138 EphB3-Fc did not reduce RRV-YFP gH-AELAAN infection, preincubation with either hPlxdc2-FcStrep or
139 a combination of hPlxdc2-FcStrep and hEphB3-Fc reduced infection by approx. 50% as observed for
140 RRV-YFP wt infection (Fig 2C). Infection of SLK cells and rhesus monkey fibroblasts was also slightly
141 decreased by preincubation of the viral inoculum with hPlxdc2-FcStrep, infection of SLK by RRV-YFP wt
142 to 63.5% ± 3.7% and infection of RF by RRV-YFP wt to 73.9% ± 11.3% relative to preincubation with
143 FcStrep as control. However, this effect was less pronounced than on HaCaT and less pronounced than
144 the effect of hPlxdc2-FcStrep on RRV-YFP gH-AELAAN infection of the same cell types (Fig 2D). Taken
145 together, the immunoprecipitation and blocking experiments confirm the independence of the
146 gH-Plxdc interaction of the previously described Eph interaction motif (23) and EphB3-binding.

147 To establish receptor function, we performed gain-of-function experiments using ectopic
148 Plxdc1/2 overexpression. Raji cells were transduced with lentiviruses encoding TwinStrep-tagged
149 human Plxdc1/2 constructs (hPlxdc1-Strep/ hPlxdc2-Strep). The EBV-positive, human lymphoblast cell

150 line only allows for low-level RRV 26-95 infection even with amounts of input virus corresponding to
151 high MOI on adherent cells like SLK, HaCaT or RF. Therefore, changes in susceptibility to infection
152 mediated by Plxdc1/2 overexpression should be readily detectable and allow for a clear differentiation
153 of the contribution of Plxdc1/2 to RRV infection over the very low intrinsic susceptibility to infection.
154 Indeed, ectopic expression of hPlxdc1/2-Strep increased RRV-YFP wt and RRV-YFP gH-AELAAN
155 infection 40 to 60-fold from approx. 0.5% basal infection dependent on the expression plasmid and
156 RRV strain (Fig 2E, G). However, we did not observe pronounced differences in effects mediated by
157 hPlxdc1-Strep or hPlxdc2-Strep, indicating no clear Plxdc receptor preference of RRV 26-95.

158 In a next step we characterized the Plxdc binding motif on RRV gH. As the RRV 17577 gH-Plxdc2
159 interaction depends on gL whereas the RRV 26-95 gH-Plxdc2 interaction does not, we focused on the
160 N-terminal domain I of gH which, in analogy to EBV gH/gL (34), most likely constitutes the gL-binding
161 interface. The differences in the Plxdc interaction of RRV isolates 26-95 and 17577 as well as the lack
162 of an interaction between KSHV gH/gL and Plxdc receptors suggested a motif that is only partially
163 conserved between the RRV isolates and missing in KSHV. Using sequence comparisons (Fig 3A) we
164 identified a putative interaction motif spanning 7 or 6 amino acid motif in the N-terminal region of RRV
165 26-95 gH and RRV 17577 gH, respectively, that is not conserved in KSHV gH. The motif is located close
166 to the Eph-interaction motif we described previously, facing in the opposite direction in a homology
167 model of the RRV 26-95 gH/gL complex based on the EBV gH/gL crystal structure (3PHF) (Fig 3B).
168 Deletion of this motif completely abrogated the gH/gL interaction with Plxdcs of both RRV 26-95 (Fig
169 3C) and RRV 17577 (Fig 3D). To further characterize the contribution of individual residues in the
170 'Tyr(Y)-Glu(E)-Tyr(Y)-Asn(N)-Glu(E)-Glu(E)-Lys(K)' (RRV 26-95) motif we performed single amino acid
171 substitutions to alanine. The ability of mutant RRV 26-95 gH-V5 to bind myc-tagged Plxdc1/2 of human
172 (hPlxdc1/2-myc) (Fig 3E) or rhesus macaque origin (mmPlxdc1/2-myc) (Fig 3F) was analyzed by
173 immunoprecipitation of gH via the V5-tag and Western blot. While several single amino acid
174 substitutions decreased the interaction of RRV gH with Plxdcs to some degree, residues Tyr23 and
175 Glu25 that are conserved in isolates 26-95 and 17577 appear to be critical for the interaction of gH

176 with human and rhesus macaque Plxdc1 and Plxdc2. Furthermore, substitution of glutamate with
177 alanine at position 22, which is not conserved between isolates 26-95 and 17577, had a pronounced,
178 albeit slightly weaker effect on the gH-Plxdc1/2 interaction (Fig 3E, F).

179 To further analyze the contribution of the gH/gL-Plxdc interaction in the context of infection
180 we constructed virus mutants deleted in the seven amino acid interaction motif in the background of
181 RRV-YFP 26-95 wildtype (RRV-YFP gHΔ21-27), and in the background of an RRV-YFP 26-95 strain
182 mutated in the Eph-interaction motif described previously by our group (RRV-YFP gH-AELAAN, RRV-
183 YFP gHΔ21-27-AELAAN) using a two-step, lambda red-mediated recombination system (35) (Fig 4A).
184 Blocking experiments using soluble hPlxdc2-FcStrep decoy receptor on HaCaT cells confirmed that
185 deletion of the seven amino acid motif was sufficient to abrogate the gH-Plxdc2 interaction on viral
186 particles (Fig 4B). While infection of RRV-YFP wt and RRV-YFP gH-AELAAN was inhibited by approx. 60%
187 to 70% respectively, infection of RRV-YFP gHΔ21-27 and RRV-YFP gHΔ21-27-AELAAN was not affected
188 even by high concentrations of soluble hPlxdc2-FcStrep (Fig 4B). All infections were carried out at
189 approx. MOI 0.05. Analogously, the Eph- or Plxdc-receptor-binding-negative RRV mutants were no
190 longer inhibited by preincubation with the respective soluble receptor (hEphB3-Fc or hPlxdc2-FcStrep)
191 in single or double inhibition experiments on HaCaT cells (Fig 4C). The receptor-specificity conveyed by
192 the respective interaction motif was further analyzed in lentiviral vector-mediated Plxdc1/2-Strep
193 overexpression experiments in Raji B lymphocytes. EphA7, which had previously been described by our
194 group to be critical for RRV infection of BJAB B lymphocytes, was used as control for Eph-mediated
195 infection. Expression of Plxdc1/2-Strep as well as EphA7-Strep dramatically enhanced susceptibility of
196 Raji cells (Fig 4D, E). RRV-YFP wt infection increased from 0.14 ± 0.04% on empty vector transduced
197 Raji cells to approx. 8.5% upon EphA7 overexpression and to approx. 17% upon Plxdc1/2
198 overexpression, without pronounced differences between the Plxdc family members. Mutation of the
199 Eph-interaction motif in RRV-YFP gH-AELAAN completely abrogated the gain in susceptibility on EphA7
200 overexpressing cells while mutation of the Plxdc-interaction motif completely abrogated the gain in
201 susceptibility on Plxdc1/2 overexpressing cells, confirming selective knockout of each individual

202 receptor interaction in the respective mutant. Furthermore, deletion of the Eph-interaction motif in
203 RRV-YFP gH-AELAAN did not impact the infection of Plxdc1/2 overexpressing cells in comparison to
204 RRV-YFP wt infection. In contrast, we observed an approx. 2-fold higher infection of RRV-YFP gHΔ21-
205 27 on EphA7 overexpression cells, when compared to RRV-YFP wt. Together, the blocking and
206 overexpression experiments indicate an independent rather than cooperative nature of Eph and Plxdc
207 receptor function.

208 To quantitatively analyze the contribution of the Plxdc1/2-interaction to RRV infection of
209 different cell types, RRV-YFP wt and RRV-YFP receptor binding mutant inocula were normalized to
210 genome copies as determined by qPCR, and target cells were inoculated with the same number of
211 encapsidated input virus genomes for wt and each mutant virus strain in an MOI range of 0.05 to 1 on
212 adherent cells. Infection as determined by the percentage of YFP+ cells was normalized to RRV-YFP wt,
213 which was set to 1. For suspension cell lines, experiments with RRV-YFP wt infection over 1% were
214 included in the analysis. Four (three for RF, five for MFB5487) independent sets of RRV wt and mutant
215 stocks were used to compensate for variability in stock preparation. None of the analyzed adherent
216 cell lines showed a preferential use of Plxdc receptors over Eph receptors based on the reduction of
217 specific infectivity of Eph-binding and Plxdc-interaction-deficient mutants (Fig 5A). On rhesus monkey
218 fibroblasts (RF), compared to RRV-YFP wt, RRV-YFP gHΔ21-27, RRV-YFP gH-AELAAN and RRV-YFP
219 gHΔ21-27-AELAAN exhibited a decrease in infection of approx. 30%, 50% and 70%, respectively.
220 Similarly on HaCaT, infection with RRV-YFP gH-AELAAN and RRV-YFP gHΔ21-27-AELAAN was reduced
221 by approx. 60% and 75%, respectively, compared to RRV-YFP wt. While RRV-YFP gHΔ21-27 exhibited a
222 defect, comparable to RRV-YFP gH-AELAAN in three of the analyzed independent sets of RRV stocks,
223 this reduction in infectivity did not reach significance due to one outlier. On SLK cells, mutation of the
224 Eph-interaction motif led to an approx. 65% decrease in infection, while RRV-YFP gHΔ21-27 infection
225 was on average comparable to RRV-YFP wt infection. In contrast, we identified B lymphocyte lines of
226 human and macaque origin that exhibit a preference in the receptor usage for either Eph or Plxdc
227 family members (Fig 5B). When normalized to genome copies, RRV-YFP gHΔ21-27 infection on human

228 Raji lymphoblasts was comparable to RRV wt infection while mutation of the Eph-interaction motif
229 lead to an approx. 90% decrease in infection, indicating preferential infection through Eph family
230 receptors, albeit at low levels, as mentioned above. Similarly, RRV-YFP gHΔ21-27 exhibited only a
231 minor defect (approx. 20% reduced infection) on immortalized B lymphocytes of macaca mulatta origin
232 (MMB1845) that did not reach significance, while infection with RRV-YFP gH-AELAAN and gHΔ21-27-
233 AELAAN was reduced by approx. 90% in comparison to RRV-YFP wt, again indicating preferential
234 infection through Eph family receptors. Conversely, deletion of the Plxdc-interaction motif decreased
235 infection of a B lymphocyte cell line of macaca fascicularis origin (MFB5487) by approx. 75% whereas
236 RRV-YFP gH-AELAAN exhibited an approx. 50% defect, indicating preferential use of the Plxdc
237 interaction for infection of MFB5487 by RRV. Mutation of both the Eph- and Plxdc-interaction motif
238 led to an even more pronounced defect of approx. 90%.

239 To evaluate the contribution of potential attachment effects on the observed differences in
240 specific infectivity, we analyzed the capacity of virions to bind Plxdc1/2 overexpressing Raji cells in
241 comparison to empty vector transduced Raji cells (Fig 5C, D). It should be noted that transduction with
242 an Plxdc1 encoding lentiviral vector resulted in drastically higher levels of protein expression as
243 assessed by Western blot analysis than transduction with an Plxdc2 encoding lentiviral vector (Fig 5C).
244 The ratio of cell-bound viral DNA to input genomes was used as a surrogate marker for virus
245 attachment. Mutation of the Plxdc- and Eph-interaction motif had no detectable effect on attachment
246 to control vector-transduced and Plxdc2-overexpressing Raji cells. In contrast, Raji cells overexpressing
247 Plxdc1 showed increased attachment of RRV-YFP wt and RRV-YFP gH-AELAAN, while attachment of
248 Plxdc-interaction negative RRV-YFPmutants gHΔ21-27 and gHΔ21-27-AELAAN was not enhanced and
249 remained comparable to empty vector control and Plxdc2-overexpressing cells.

250 To exclude effects of potential offsite genomic rearrangements in RRV-YFP gHΔ21-27 we
251 created two independent revertants (RRV-YFP gHΔ21-27^{rev9-4} and RRV-YFP gHΔ21-27$^{rev10-3}$).
252 Restoration of the residues deleted in RRV-YFP gHΔ21-27 restored infection on hPlxdc1/2-transduced
253 Raji, MFB5487 and HaCaT cells to RRV-YFP wt levels, with no pronounced differences between RRV-

254 YFP wt, RRV-YFP gHΔ21-27^{rev9-4} and RRV-YFP gHΔ21-27$^{rev10-3}$ (Fig 5E). Similar to the approx. 11-fold
255 increase of RRV-YFP wt infection upon hPlxdc1/2 overexpression, infection with RRV-YFP gHΔ21-27
256 revertants increased from 2.00% ± 0.30% (2.54% ± 0.29%) on empty vector transduced Raji cells to
257 35.25% ± 1.21% (36.99% ± 0.39%) and 37.27% ± 0.68% (43.00% ± 0.99%) upon hPlxdc1 and hPlxdc2
258 overexpression for RRV-YFP gHΔ21-27^{rev9-4} (RRV-YFP gHΔ21-27$^{rev10-3}$), respectively (Fig 5E).

259 Our interaction data (Fig 1A, B) suggests that at least RRV 26-95 gH can bind Plxdc1/2 in the
260 absence of gL. We therefore aimed to analyze if infection with a RRV 26-95 gL deletion mutant (RRV-
261 YFP ΔgL) is influenced by Plxdc1 and 2 expression to a similar degree as RRV-YFP wt and RRV-YFP gH-
262 AELAAN infection. As shown before, overexpression of hEphA7-Strep or hPlxdc1/2-Strep in Raji cells
263 dramatically increased RRV-YFP wt infection compared to empty vector transduced cells (22-fold for
264 hEphA7-Strep, 23-fold for hPlxdc2-Strep and 26-fold for hPlxdc2-Strep) (Fig 6). RRV-YFP gH-AELAAN
265 infection was increased from 0.25% ± 0.05% basal infection on empty vector transduced cells to
266 52.53% ± 2.06% and 65.5% ± 1.22%, respectively, upon hPlxdc1-Strep or hPlxdc2-Strep overexpression,
267 while hEphA7-Strep overexpression had no pronounced effect on infection. We observed a pattern
268 similar to RRV-YFP gH-AELAAN for the infection with two independent RRV-YFP ΔgL clones, RRV-YFP
269 ΔgL$^{3-3}$ and RRV-YFP ΔgL$^{3-5}$. While, hEphA7-Strep overexpression did not influence RRV-YFP ΔgL
270 infection, hPlxdc1/2-Strep overexpression enhanced infection from 0.36% ± 0.03% (0.48% ± 0.04%) on
271 empty vector transduced Raji cells to 31.05% ± 0.95% (36.25% ± 1.42%) and 35.59% ± 0.94% (42.55%
272 ± 0.57%) upon hPlxdc1 and hPlxdc2 overexpression for RRV-YFP ΔgL$^{3-3}$ (RRV-YFP ΔgL$^{3-5}$) respectively
273 (Fig 6C). Even though the effect of Plxdc1/2 overexpression on RRV-YFP ΔgL infection was slightly less
274 pronounced than the effect on RRV-YFP wt and RRV-YFP gH-AELAAN infection, this data demonstrates
275 that the use of Plxdc1 and Plxdc2 as RRV 26-95 entry receptors is possible in a gL-independent manner.

276 **DISCUSSION**

277 In this study we identified the Plexin domain containing proteins 1 and 2 as a novel family of
278 entry receptors for RRV. Plxdc1/2 interact with the gH/gL complex of RRV in a region close to the

279 previously characterized binding motif for Eph receptors. While the Eph-interaction as well as the
280 critical Eph binding motif in domain I of gH is conserved between RRV and the closely related human
281 pathogenic KSHV (23), the interaction with Plxdc1/2 is exclusive to RRV and even exhibits differences
282 between isolates 26-95 and 17577 as prototypic members of the two described RRV sequence clades.
283 According to our results, differences between Plxdc1 and Plxdc2 may also exist in terms of
284 function. While overexpression of both Plxdc1 and Plxdc2 in Raji cells, that were virtually "non-
285 susceptible" under the conditions used, lead to robust RRV 26-95 infection (Fig 4D-E), only
286 overexpression of Plxdc1 enhanced attachment of RRV wt and RRV gH-AELAAN in comparison to either
287 non-transduced Raji cells or Plxdc-binding deficient RRV mutants (Fig 5D). Whether this is primarily
288 due to differences in expression levels, consistently observed between Plxdc1 and Plxdc2 upon
289 lentiviral overexpression or due to underlying functional differences in the gH interaction with these
290 molecules remains to be determined.
291 Mutation of residues Tyr23 and Glu25 in gH domain I, which are conserved between RRV
292 isolate 26-95 and 17577, almost abolished the interaction with Plxdc2, which is bound by gH/gL of both
293 isolates. Although the same residues are critical for the interaction of RRV gH 26-95 with Plxdc1, the
294 partial conservation of the region appears to be insufficient to confer binding of 17577 gH to Plxdc1.
295 Interestingly, the interaction of 17577 gH with Plxdc2 is dependent on the presence of gL in the gH/gL
296 complex, whereas 26-95 gH is able to bind Plxdc1/2 independent of gL. These features of Plxdc1/2
297 binding specificities appear similar to the interaction of the gH/gL complex with Eph receptors, wherein
298 mutation of the strictly conserved Eph interaction motif is sufficient to abrogate receptor binding, but
299 differences in KSHV and RRV affinities for A- and B-type Eph RTKs indicate the existence of additional
300 regions in gH or gL that contribute to or modulate the interaction. Whether these preferences for
301 different members of conserved receptor families also influence e.g. cell or tissue tropism, viral spread
302 or pathogenicity has not been determined. Sequence comparisons of over twenty RRV isolates
303 identified dramatic differences in the extracellular domains of gH as well as in gL between isolates that
304 fell in two discrete groupings either similar to 26-95 or 17577, while variation in other glycoproteins

305 R1, gM, gN, orf68 was minimal between clades (4). However, if these clade-specific glycoprotein
306 variations influence the observed differences in pathogenicity between RRV strains 26-95 and 17577
307 remains to be seen. Another interesting question would be if the receptor-binding function of the N-
308 terminal region of gH is conserved between RRV and KSHV, and probably EBV, and whether KSHV and
309 EBV can bind another receptor through this region. So far, we did not identify corresponding
310 interactions for KSHV, but in principle the region of gH encompassing the Plxdc2 binding site is present
311 in both viruses and it is tempting to assume some functional conservation.

312 Along those lines, the evolutionary factors that drive interaction with different receptor
313 families and the resulting multitude of herpesvirus–receptor interactions is highly interesting. For e.g.
314 EBV and HCMV, a clear correlation between receptor usage, dependent on viral interaction partners
315 of the gH/gL complex, and cell tropism has been demonstrated in various studies ((36), reviewed in
316 (37)). However, for rhadinoviruses, the picture is less clear. We demonstrate that RRV infection of
317 select cell lines exhibited a dependence on specific receptors, e.g. Raji infection – to the modest extent
318 that was possible without recombinant receptor overexpression – was dependent on the gH/gL-Eph
319 interaction, MFB5487 infection was more dependent on the Plxdc-interaction (Fig 5), and similarly
320 mutation of the Eph-interaction motif did not impact infection on all cell types equivalently (23). Yet,
321 a definite correlation between exclusive receptor usage and infection of specific cell types is not
322 obviously apparent. While the notion of a role of different receptor interactions in KSHV and RRV cell
323 and tissue tropism is tempting and an established concept for related viruses (37–39), the possibility
324 of a redundant function should not be discarded. Redundancy could be driven by the need to escape
325 antibodies e.g. to one receptor binding site. For instance, *in vitro* infection of human keratinocytes or
326 rhesus fibroblasts seemed to be impacted to a similar degree by either deletion of the Eph- or of the
327 Plxdc-interaction motif (Fig 5). To ultimately address the correlation between receptor- and tissue-
328 tropism, *in vivo* studies using receptor-de-targeted mutants to analyze cell and tissue tropisms will be
329 required. The importance of *in vivo* studies is also supported by a recent report that showed that a gL-
330 null RRV mutant still established persistent infection in the B cell compartment upon intravenous

331 inoculation, while infection of B cells *in vitro* was drastically reduced (24), a finding that could be
332 explained by the gL-independent usage of Plxdc1/2 for B cell infection *in vivo.* At a minimum, our data
333 on RRV-YFP ΔgL infection of Plxdc1 and Plxdc2 overexpressing Raji cells (Fig 6) confirms that RRV can
334 efficiently use Plxdc1 and Plxdc2 as entry receptors in the absence of gL. Finally, the fact that a mutant
335 that was deleted in both the Eph and the Plxdc1/2 interaction motif, RRV-YFP gHΔ21-27-AELAAN, was
336 still able to replicate on rhesus monkey fibroblasts, as evidenced by the fact that we were able to grow
337 a virus stock on these cells, and was still infectious to a certain degree on a number of cell lines (Figs 4
338 and 5) indicates a surprisingly high degree of redundancy in the entry pathways that RRV can use and
339 hints at the existence of additional receptors or host factors besides Ephs and Plexin domain containing
340 proteins.

341 On a more speculative note, the apparent overlap between virus receptors and tumor-
342 associated membrane proteins may represent an interesting research subject. Eph receptors were first
343 identified in an attempt to characterize tyrosine kinases involved in cancer (40) and altered expression
344 in various cancer types has been demonstrated for several Eph family members (reviewed in (41)).
345 Similarly, Plxdc1 was first described in a screen for novel tumor endothelial members (25) and
346 expression of both Plxdc1 and Plxdc2 is elevated in the endothelium of solid tumors (25, 26, 42, 43).
347 Plxdc1 expression has been described as prognostic marker and modulating factor for various human
348 cancers (42–46). Given the overlap between the required changes e.g. in metabolism, transcription,
349 and signaling for cancer growth and virus replication it seems not unlikely that either elevated
350 expression or signaling of these molecules is favorable for both virus infection and cancer progression.
351
352
353
354
355
356

357 **FIGURES**

358

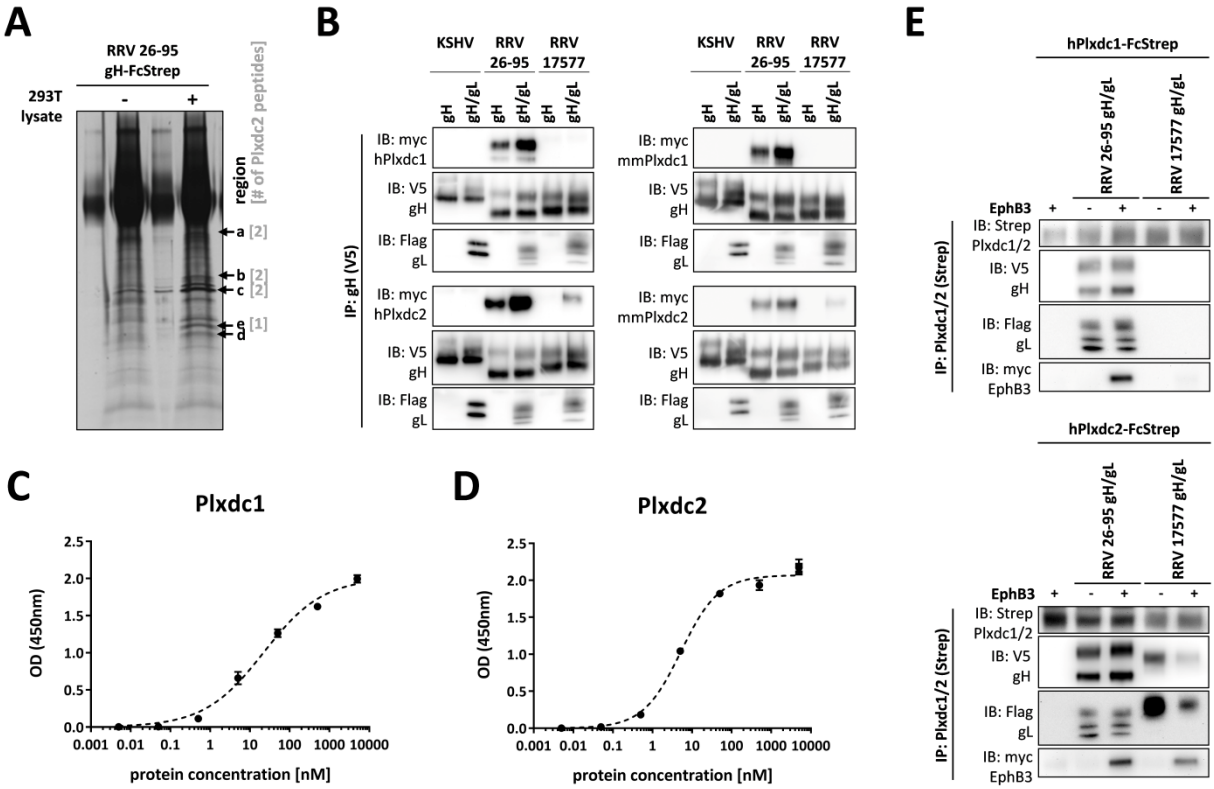

359

360 **Figure 1 Plxdc family receptors are novel interaction partners for the RRV gH/gL**. **A)**
361 Immunoprecipitation of recombinant soluble RRV 26-95 gH-FcStrep in the presence or absence of 293T
362 lysate. Precipitates were analyzed by PAGE, silver stained and bands at the indicated molecular weight
363 (arrows, regions a-d) were excised and analyzed by mass spectrometry. Numbers in brackets indicate
364 the number of Plxdc2 peptides identified by LC-MS/MS in each region. **B)** V5-tagged RRV 26-95 gH, RRV
365 17577 gH or KSHV gH alone or co-expressed with the respective Flag-tagged gL construct were
366 immunoprecipitated in the presence of full-length Plxdc1 or Plxdc2 from human (h) or macaca mulatta
367 (mm) origin using monoclonal antibody to the V5-tag. Precipitates were analyzed by Western blot with
368 the indicated antibodies. **C-D)** Binding of Plxdc1 ectodomain C) or Plxdc2 ectodomain D) at various
369 concentrations to immobilized RRV 26-95 gH-FcStrep/gL was measured by enzyme-linked
370 immunosorbent assay. Curve Fitting and determination of half-maximal binding concentration was
371 performed based on the *One site specific binding with Hill Slope equation* in Prism6. **E)** Co-

372 immunoprecipitation of soluble human Plxdc1-FcStrep or human Plxdc2-FcStrep with RRV 26-95 gH-
373 V5/gL-Flag or RRV 17577 gH-V5/gL-Flag using StrepTactin Sepharose in the presence or absence of
374 human full-length EphB3. Abbreviations: IP: immunoprecipitation, IB: immunoblotting, h: human, mm:
375 macaca mulatta (rhesus macaque).

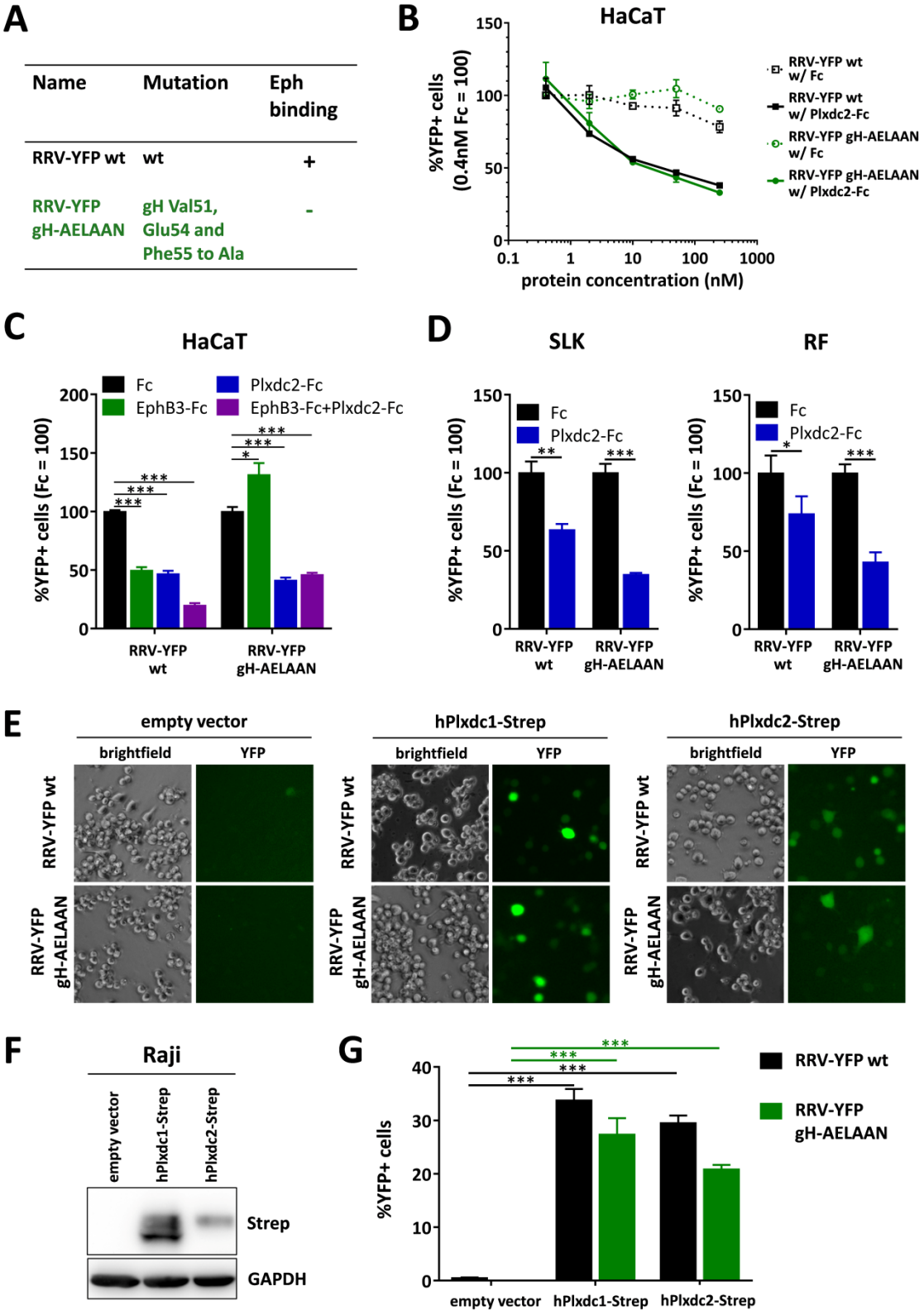

Figure 2 Plxdc1/2 function as entry receptors for RRV. A) List of BAC-derived recombinant viruses and introduced mutations used in this figure. **B)** Dose-dependent inhibition of RRV 26-95 infection by soluble human Plxdc2-FcStrep on HaCaT cells. RRV-YFP wt and RRV-YFP gH-AELAAN were pre-

380 incubated with hPlxdc2-FcStrep for 30min at room temperature. FcStrep alone was used as control.
381 YFP expression as indicator of infection was measured by flow cytometry. Infection in the presence of
382 0.4nM FcStrep was set to 100% (MOI ~0.2, triplicates, error bars represent SD). **C)** Inhibition of RRV 26-
383 95 infection by soluble Plxdc2-FcStrep and EphB3-Fc on HaCaT cells. RRV-YFP wt and RRV-YFP gH-
384 AELAAN were pre-incubated with 100nM hPlxdc2-FcStrep, 10nM EphB3-Fc or a combination of 100nM
385 hPlxdc2-FcStrep and 10nM EphB3-Fc for 30min at room temperature. FcStrep alone was used as
386 control. YFP expression as indicator of infection was measured by flow cytometry. Infection with
387 FcStrep was set to 100% (MOI ~0.2, triplicates, error bars represent SD). **D)** Inhibition of RRV 26-95
388 infection by soluble human Plxdc2-FcStrep on SLK cells and rhesus fibroblasts. RRV-YFP wt and RRV-
389 YFP gH-AELAAN were pre-incubated with 250nM hPlxdc2-FcStrep for 30min at room temperature.
390 FcStrep alone was used as control. YFP expression as indicator of infection was measured by flow
391 cytometry. Infection with FcStrep was set to 100% (MOI ~0.05-0.1, triplicates, error bars represent SD).
392 **E)** Raji cells were transduced with TwinStrep-tagged human Plxdc1 and Plxdc2 (hPlxdc1-Strep/ hPlxdc2-
393 Strep) expression constructs or an empty vector control, briefly selected and infected with RRV-YFP wt
394 or RRV-YFP gH-AELAAN normalized to genome copies as determined by qPCR. Micrographs show
395 representative infection of the indicated cell pools. **F)** Lysates of transduced Raji cell pools were
396 analyzed for Plxdc1/2-Strep expression by Western blot. **G)** Quantification of (E) by flow cytometric
397 analyses of YFP reporter gene expression as indicator of infection.

398

399

400

401

402

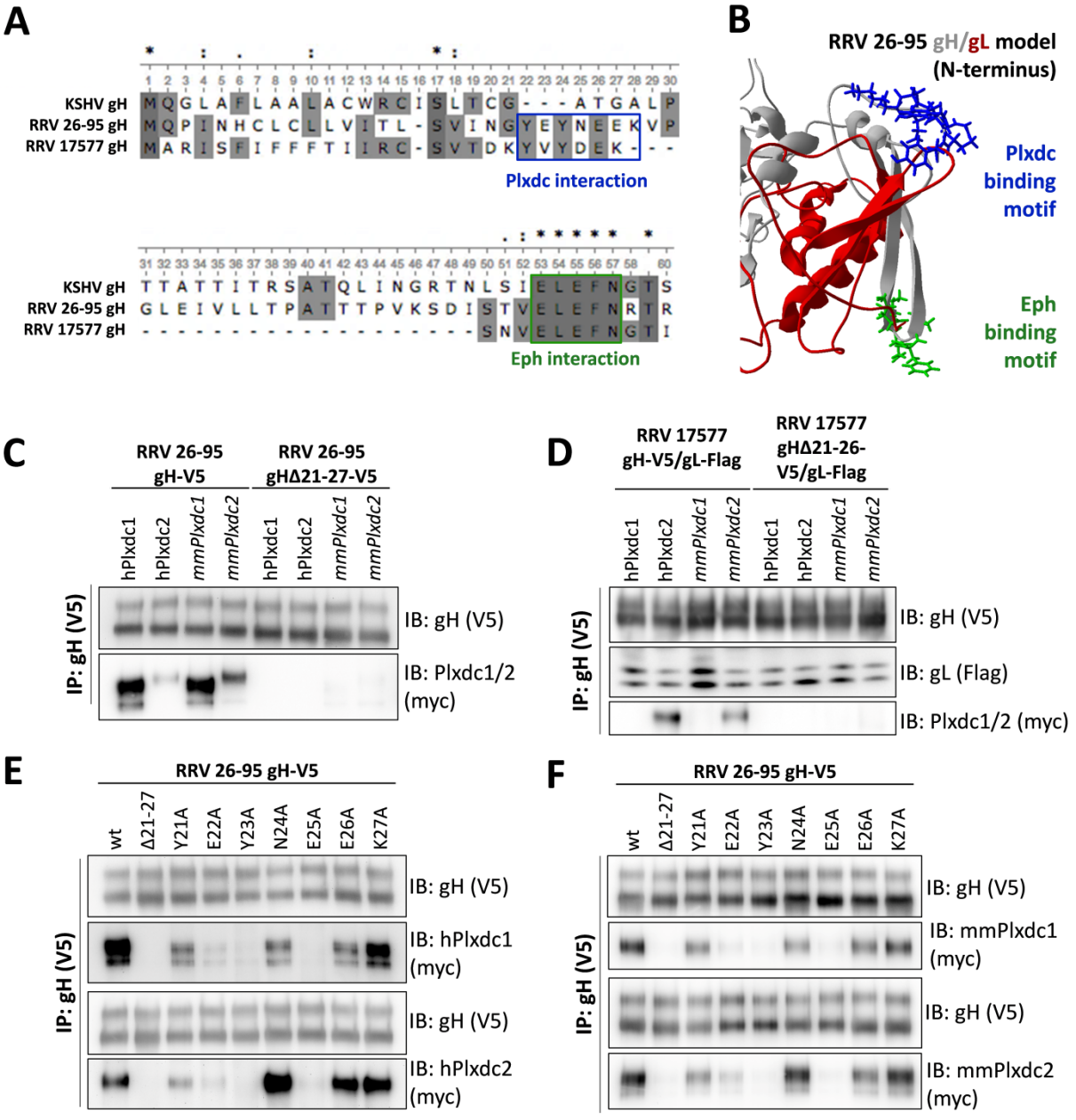

Figure 3 An amino acid sequence motif in the N-terminal region of RRV 26-95 and RRV 17577 gH is essential for the Plxdc interaction. A) Multiple sequence alignment of the N-terminal region of gH of KSHV and the two RRV isolates 26-95 and 17577. Boxes indicate the binding motives for Eph receptors (green) and Plxdc receptors (blue). **B)** Homology-based structure prediction of the RRV 26-95 gH/gL complex based on the crystal structure of the EBV gH/gL complex (PDB number 3PHF) using the Iterative Threading ASSembly Refinement (I-TASSER) server and the CO-THreader (COTH) algorithms for protein-protein complex structure and multi-chain protein threading. The Eph receptor interaction motif is shown in green, the Plxdc interaction motif is shown in blue, gL is shown in red, gH is shown in

412 grey. **C)** Deletion of the Plxdc interaction motif in RRV 26-95 gH (amino acid 21-27, "YEYNEEK")
413 abrogates gH interaction with Plxdc1 and Plxdc2. V5-tagged gH wt or gHΔ21-27 were
414 immunoprecipitated in the presence of full-length human or macaca mulatta Plxdc1-myc or Plxdc2-
415 myc using monoclonal antibody to the V5-tag. Precipitates were analyzed by Western blot. **D)** Deletion
416 of the Plxdc interaction motif in RRV 17577 gH (amino acid 21-26, "YVYDEK") abrogates gH interaction
417 with Plxdc2. V5-tagged gH wt or gHΔ21-26 was co-expressed with Flag-tagged RRV 17577 gL. gH-
418 V5/gL-Flag complexes were immunoprecipitated in the presence of full-length human or macaca
419 mulatta Plxdc1-myc or Plxdc2-myc using monoclonal antibody to the V5-tag. Precipitates were
420 analyzed by Western blot. **E)** Mutational scan of Plxdc interaction motif (amino acid 21-27, "YEYNEEK")
421 of RRV 26-95 gH identifies human Plxdc1/2-interacting residues. V5-tagged gH mutants were
422 immunoprecipitated in the presence of full-length human Plxdc1-myc or Plxdc2-myc using monoclonal
423 antibody to the V5-tag. Precipitates were analyzed by Western blot. RRV gHΔ21-27 serves as negative
424 control. **F)** Mutational scan of Plxdc interaction motif (amino acid 21-27, "YEYNEEK") of RRV 26-95 gH
425 identifies rhesus macaque Plxdc1/2-interacting residues. V5-tagged gH mutants were
426 immunoprecipitated in the presence of full-length human Plxdc1-myc or Plxdc2-myc using monoclonal
427 antibody to the V5-tag. Precipitates were analyzed by Western blot. RRV gHΔ21-27 serves as negative
428 control. Abbreviations: IP: immunoprecipitation, IB: immunoblotting, h: human, mm: macaca mulatta
429 (rhesus macaque).

430

431

432

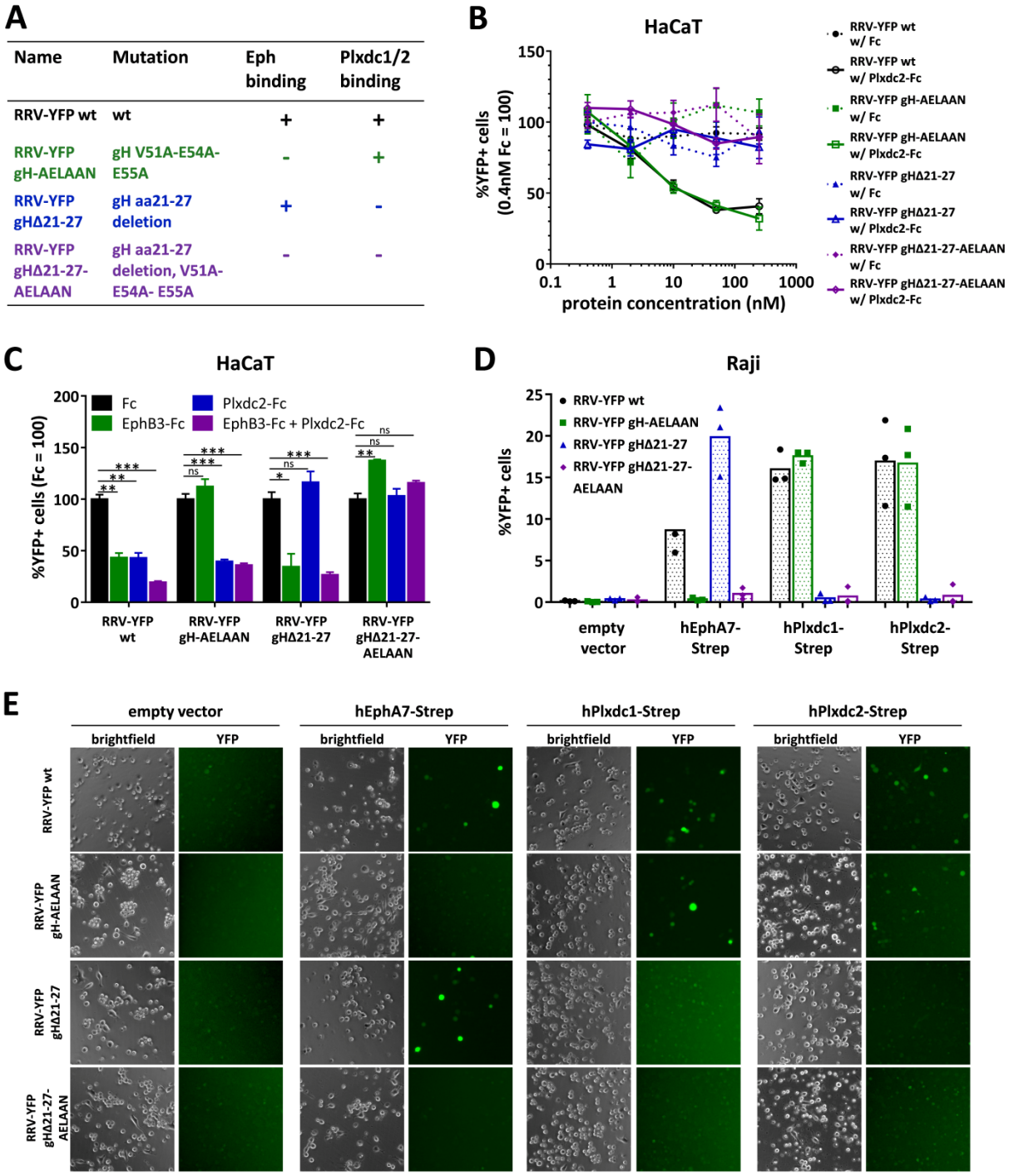

Figure 4 Deletion of the seven amino acid Plxdc-binding motif is sufficient to detarget RRV 26-95 from Plxdc receptors A) List of BAC-derived recombinant viruses and introduced mutations used in this figure. **B)** Dose-dependent inhibition of RRV 26-95 infection by soluble human Plxdc2-FcStrep on HaCaT cells. RRV-YFP wt, RRV-YFP gH-AELAAN, RRV-YFP gHΔ21-27 and RRV-YFP gHΔ21-27-AELAAN were pre-incubated with hPlxdc2-FcStrep for 30min at room temperature. FcStrep alone was used as control. YFP expression as indicator of infection was measured by flow cytometry. Infection in the

440 presence of 0.4nM FcStrep was set to 100% (MOI ~0.05, triplicates, error bars represent SD). **C)**
441 Inhibition of RRV 26-95 infection by soluble Plxdc2-FcStrep and EphB3-Fc on HaCaT cells. RRV-YFP wt,
442 RRV-YFP gH-AELAAN, RRV-YFPgHΔ21-27 and RRV-YFP gHΔ21-27-AELAAN were pre-incubated with
443 100nM hPlxdc2-FcStrep, 10nM EphB3-Fc or a combination of 100nM hPlxdc2-FcStrep and 10nM
444 EphB3-Fc for 30min at room temperature. FcStrep alone was used as control. YFP expression as
445 indicator of infection was measured by flow cytometry. Infection with FcStrep was set to 100% (MOI
446 ~0.1-0.2, triplicates, error bars represent SD). **D)** Raji cells were transduced with TwinStrep-tagged
447 human EphA7, Plxdc1 or Plxdc2 (hEphA7-Strep, hPlxdc1-Strep, hPlxdc2-Strep) expression constructs or
448 an empty vector control, briefly selected and infected with RRV-YFP wt, RRV-YFP gH-AELAAN, RRV-YFP
449 gHΔ21-27 or RRV-YFP gHΔ21-27-AELAAN normalized to genome copies as determined by qPCR. YFP
450 expression as indicator of infection was measured by flow cytometry. The mean across three
451 independent sets of RRV stocks is indicated by columns. The means of individual triplicate infections
452 for each set of RRV stocks are given as symbols within the respective columns. **E)** Micrographs show
453 representative infection of one set of RRV stocks in (D).

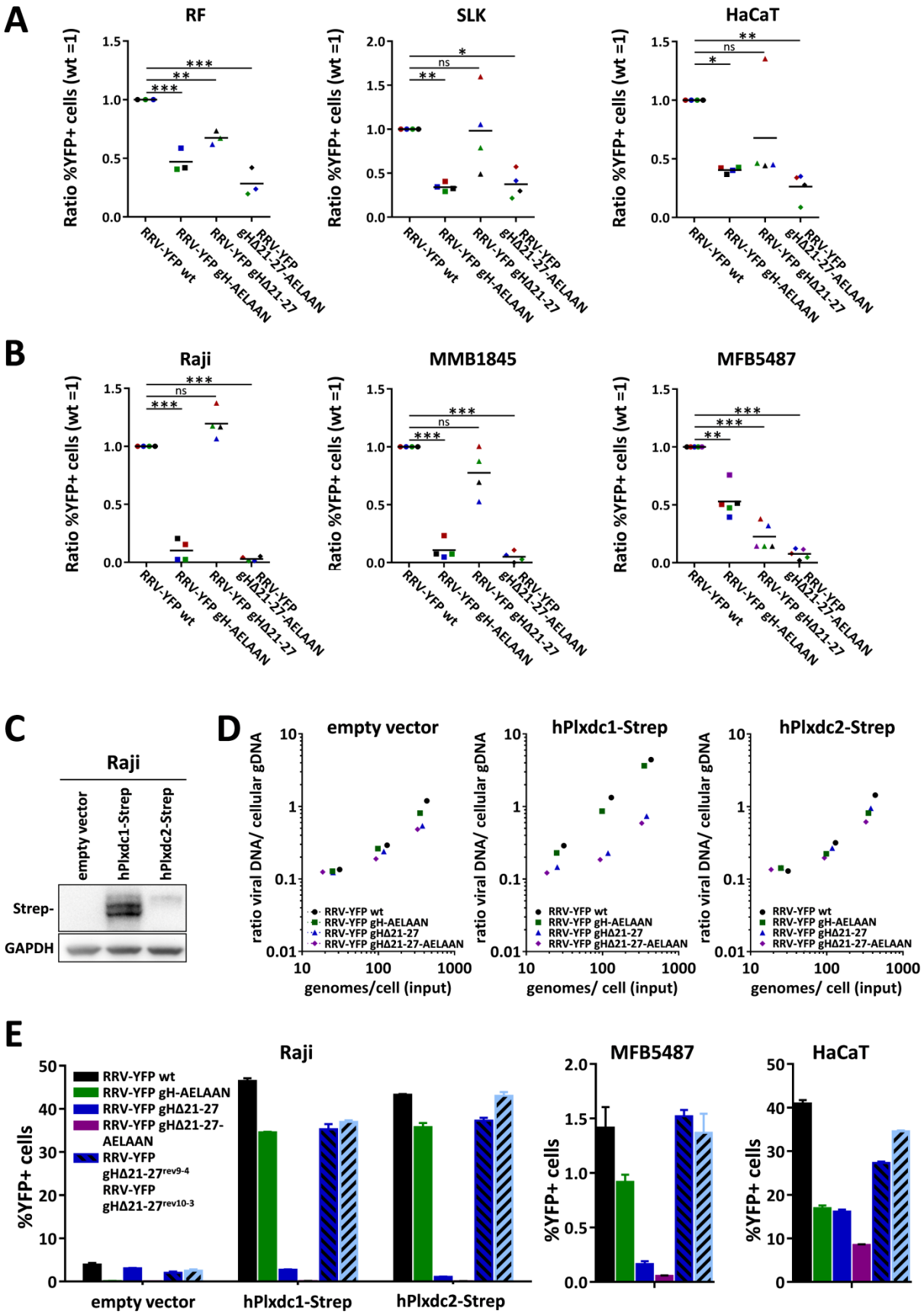

454

455 **Figure 5 The contribution of the RRV 26-95 gH-Plxdc interaction to infection is cell type-specific and**

456 **may in part be dependent on attachment effects. A)** RRV 26-95 deleted in the Plxdc interaction motif

457 exhibits reduced specific infectivity on HaCaT and RF, but not SLK cells. Target cells were infected with
458 RRV-YFP wt, RRV-YFP gH-AELAAN, RRV-YFP gHΔ21-27 or RRV-YFP gHΔ21-27-AELAAN normalized to
459 genome copies as determined by qPCR. YFP expression as indicator of infection was measured by flow
460 cytometry and normalized to RRV-YFP wt infection. Means of individual normalized infections with
461 three (RF) or four (HaCaT, SLK) independent sets of RRV stocks are given as symbols of different color.
462 Sets with RRV-YFP wt infection in an MOI range of 0.05 - 1 were used for analysis. The mean across the
463 independent sets of RRV stocks is indicated by black lines. **B)** RRV 26-95 deleted in the Plxdc interaction
464 motif exhibits reduced specific infectivity on MFB5487, but not Raji and MMB1845 cells. Target cells
465 were infected with RRV-YFP wt, RRV-YFP gH-AELAAN, RRV-YFP gHΔ21-27 or RRV-YFP gHΔ21-27-
466 AELAAN normalized to genome copies as determined by qPCR. YFP expression as indicator of infection
467 was measured by flow cytometry and normalized to RRV-YFP wt infection. Means of individual
468 normalized infections with four (Raji, MMB1845) or five (MFB5487) independent sets of RRV stocks
469 are given as symbols of different color. Sets with RRV-YFP wt infection exceeding 1% were used for
470 analysis. The maximal achieved RRV-YFP wt infection was 6.1% for Raji, 5.6% for MMB1845 and 3.1%
471 for MFB5487, respectively. The mean across the independent sets of RRV stocks is indicated by black
472 lines. **C)** Western blot analysis of Raji cells transduced with TwinStrep-tagged human Plxdc1 and Plxdc2
473 (hPlxdc1-Strep/ hPlxdc2-Strep) expression constructs or an empty vector control. **D)** Attachment of
474 RRV 26-95 on transduced Raji cells is affected by hPlxdc1-Strep, but not hPlxdc2-Strep overexpression.
475 Cells, analyzed in (C), were incubated with cold virus at the indicated concentrations at 4°C for 30min
476 followed by genomic DNA isolation. The ratio of viral to cellular DNA as measurement for attached
477 virus was calculated based on ΔCt values of a genomic (CCR5) and a viral locus (ORF73/ LANA) as
478 determined by qPCR and plotted against input viral genome number. **E)** Re-introduction of the seven
479 amino acid motif crucial for Plxdc interaction rescues RRV-YFPgHΔ21-27 infection. Transduced Raji
480 cells, analyzed in (C), MFB5487 and HaCaT cells were infected with RRV-YFP wt, RRV-YFP gH-AELAAN,
481 RRV-YFP gHΔ21-27, RRV-YFP gHΔ21-27-AELAAN or two RRV-YFP gHΔ21-27 revertants (RRV-YFP gHΔ21-

482 27^{rev9-4}, RRV-YFPgHΔ21-$27^{rev10-3}$) normalized to genome copies as determined by qPCR. YFP expression

483 as indicator of infection was measured by flow cytometry (triplicates, error bars represent SD).

484

485

486

487

488

489

490

491

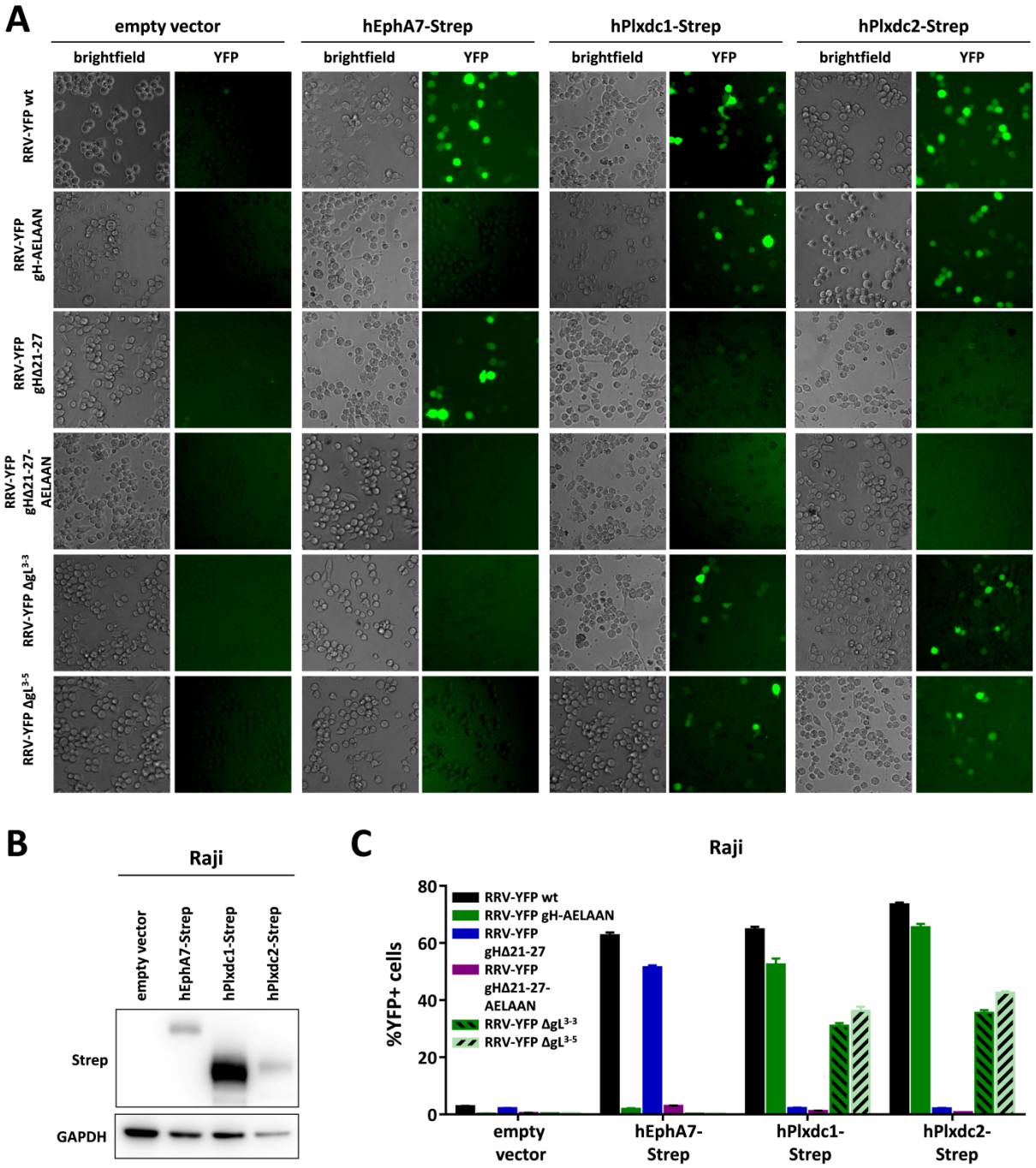

Figure 6 Plxdc1/2-dependent infection with RRV 26-95 does not require gL. A) Raji cells were transduced with TwinStrep-tagged human EphA7, Plxdc1 and Plxdc2 (hEphA7-Strep/ hPlxdc1-Strep/ hPlxdc2-Strep) expression constructs or an empty vector control, briefly selected and infected with RRV-YFP wt or RRV-YFP gH-AELAAN, RRV-YFP gHΔ21-27 or one of two RRV-YFP ΔgL clones normalized to genome copies as determined by qPCR. Micrographs show representative infection of the indicated cell pools. **B)** Lysates of transduced Raji cell pools were analyzed for EphA7-Strep and Plxdc1/2-Strep

499 expression by Western blot. **C)** Quantification of (A) by flow cytometric analyses of YFP reporter gene
500 expression as indicator of infection (triplicates, error bars represent SD).

501 **MATERIAL AND METHODS**

502 **Cells.** Human embryonic kidney (HEK) 293T cells (RRID:CVCL_0063) (laboratory of Tobias Moser), SLK cells
503 (RRID:CVCL_9569) (NIH AIDS Research and Reference Reagent program), rhesus monkey fibroblasts (RF)
504 (laboratory of Prof. Rüdiger Behr) and HaCaT human keratinocytes (RRID:CVCL_0038) were cultured in
505 Dulbecco's Modified Eagle Medium (DMEM), high glucose, GlutaMAX, 25mM HEPES (Thermo Fisher Scientific)
506 supplemented with 10% fetal calf serum (FCS) (Thermo Fisher Scientific), and 50µg/ml gentamycin (PAN Biotech).
507 iSLK cells (laboratory of Don Ganem, Novartis Institutes for BioMedical Research, Emeryville, CA, USA) were
508 maintained in DMEM supplemented with 10% FCS, 50µg/ml gentamycin, 2.5µg/ml puromycin (InvivoGen) and
509 250µg/ml G418 (Carl Roth). Raji cells (RRID:CVCL_0511) (laboratory of Jens Gruber), MFB5487 (a clonal cell line
510 established from macaca fascicularis PBMC, immortalized by infection with herpesvirus papio; a kind gift from
511 Ulrike Sauermann) and MMB1845 cells (a clonal cell line established from macaca mulatta PBMC, immortalized
512 by infection with herpesvirus papio; a kind gift from Ulrike Sauermann) were cultured in RPMI (Thermo Fisher
513 Scientific) supplemented with 10% FCS and 50µg/ml gentamycin.
514

515 **BAC mutagenesis and virus production.** RRV recombinants (RRV-YFP gHΔ21-27, RRV-YFP ΔgL and RRV-YFP
516 gHΔ21-27-AELAAN) were generated based on BAC35-8 (47) and RRV gH-AELAAN (23) respectively, using a two-
517 step, markerless λ-red-mediated BAC recombination strategy as described by Tischer et al. (35). RRV-YFP ΔgL
518 harbors a 128 bp deletion, which introduces a frameshift after amino acid 26 and a stop codon after amino acid
519 37, leaving only six amino acids of the original gL sequence after the putative signal peptide cleavage site. RRV-
520 YFP gHΔ21-27 revertants were generated based on RRV-YFP gHΔ21-27 following the same protocol described by
521 Tischer et al. (35). In short, recombination cassettes were generated from the pEPKanS template by polymerase
522 chain reaction (PCR) with Phusion High Fidelity DNA polymerase (Thermo Fisher Scientific) using long
523 oligonucleotides (Ultramers; purchased from Integrated DNA Technologies (IDT)) (see S1 Table for a complete
524 list of primers). Recombination cassettes were transformed into RRV-YFP-carrying GS1783 followed by
525 kanamycin selection, and subsequent second recombination under 1% L(+)arabinose (Sigma-Aldrich)-induced I-
526 SceI expression. Colonies were verified by PCR of the mutated region followed by sequence analysis (Macrogen),

527 pulsed-field gel electrophoresis and restriction fragment length polymorphism. For this purpose, bacmid DNA
528 was isolated by standard alkaline lysis from 5ml liquid cultures. Subsequently, the integrity of bacmid DNA was
529 analyzed by digestion with restriction enzyme *Xho*I and separation in 1% PFGE agarose (Bio-Rad) gels and 0.5×TBE
530 buffer by pulsed-field gel electrophoresis at 6 V/cm, 120-degree field angle, switch time linearly ramped from 1s
531 to 5s over 16 h (CHEF DR III, Bio-Rad). Infectious RRV-YFP recombinants were generated as described previously
532 (23). In short, bacmid DNA (NucleoBond Xtra Midi) was transfected into 293T cells using GenJet Ver. II (Signagen)
533 according to manufacturer's instructions. Transfected 293T cells were transferred onto a confluent rhesus
534 monkey fibroblasts monolayer two days after transfection and co-cultivated until a visible cytopathic effect (CPE)
535 was observed. For virus stocks preparations, confluent primary rhesus monkey fibroblasts were inoculated with
536 infectious supernatant of 293T/rhesus monkey fibroblast co-cultures. After multiple rounds of replication virus-
537 containing RF supernatant was clarified by centrifugation (4750g, 10 minutes), concentrated by overnight
538 centrifugation (4200rpm, 4°C) and careful aspiration of approximately 95% of the supernatant. The pellet was
539 resuspended overnight in the remaining liquid. Stocks of wt and recombinant viruses were aliquoted and stored
540 at -80°C. Mutations were verified by PCR amplification of the respective region followed by sequence analysis
541 (Macrogen).
542
543 **Plasmids.** The pcDNA4 vector containing full-length EphB3 (ref|BC052968|, pcDNA-EphB3-myc), pcDNA6aV5
544 vectors containing RRV/KSHV gH and gL coding sequences (ref|GQ994935.1|, pcDNA6aV5-KSHV-gH, pcDNA3.1-
545 KSHV-gL-Flag (14); ref|AF210726.1|, pcDNA6aV5-RRV-26-95-gH, pcDNA3.1-RRV-26-95-gL-Flag (15, 48);
546 ref|AF083501.3|, pcDNA6aV5-RRV-17577-gH, pcDNA3.1-RRV-17577-gL-Flag (15)) were described elsewhere.
547 RRV 26-95/ RRV 17577 recombinant gH constructs were generated based on pcDNA6aV5-RRV-26-95-gH or
548 pcDNA6aV5-RRV-17577-gH, respectively, using 'Round the Horn Site-directed mutagenesis. Expression plasmids
549 pcDNA4-hPlxdc1-myc (Homo sapiens, full-length, ref |NM_020405.5|) and pcDNA4-hPlxdc2-myc (Homo sapiens,
550 full-length, ref |NM_032812.9|) were generated by PCR based restriction cloning. The soluble ectodomain of
551 human Plxdc2 (amino acids 31-453) without signal peptide was inserted behind a heterologous signal peptide of
552 murine IgG-kappa into pAB61Strep by PCR based restriction cloning, resulting in a C-terminally fused IgG1 Fc-
553 fusion protein with a C-terminal tandem Strep-Tag (pPlxdc2-FcStrep) as described previously (49). pcDNA6
554 vectors constructs containing human Plxdc1 ectodomain (aa 1-425) with a 6XHis Tag (pcDNA6-ectoPlxdc1-6XHis)
555 or human Plxdc2 ectodomain (aa 1-453) with a 6XHis Tag (pcDNA6-ectoPlxdc2-6XHis) were based on pcDNA4-

556 hPlxdc1-myc/ pcDNA4-hPlxdc2-myc, which were PCR-amplified and ligated using exonuclease-based Gibson-
557 assembly (Gibson Assembly Mastermix, New England Biolabs). Expression plasmids pcDNA4-mmPlxdc1-myc
558 (macaca mulatta, full-length, ref |XM_028836436.1|) and pcDNAmmPlxdc2-myc (macaca mulatta, full-length,
559 ref |XM_028826043.1|) were generated based on PCR-amplified gBlock gene fragments (purchased from IDT)
560 of the regions varying from human Plxdc1 (nt1-1200) and Plxdc2 (nt1-1401), respectively, and ligated in the
561 respective PCR-amplified backbone (pcDNA4hPlxdc1-myc, pcDNA4hPlxdc2-myc) by exonuclease-based Gibson .
562 pLenti CMV Blast DEST (706-1) (a gift from Eric Campeau & Paul Kaufman (Addgene plasmid #17451)) constructs
563 carrying a human Plxdc1-TwinStrep or Plxdc2-TwinStrep expression cassette (pLenti-CMV-Blast-Plxdc1-Strep/
564 pLenti-CMV-Blast-Plxdc2-Strep) were based on pcDNA4-hPlxdc1-myc/ pcDNA4-hPlxdc2-myc, which were PCR-
565 amplified and ligated using exonuclease-based Gibson-assembly. pLenti-CMV-Blast-EphA7-Strep was described
566 before (20). (See S1 Table for a complete list of primers and constructs).
567

568 **Recombinant proteins.** Recombinant, soluble FcStrep and Plxdc2-FcStrep-fusion proteins were purified under
569 native conditions by Strep-Tactin chromatography from 293T cell culture supernatant. 293T cells were
570 transfected with pAB61Strep or pPlxdc2-FcStrep using Polyethylenimine "Max" (PEI) (Polysciences) (50) as
571 described before (20) with pAB61Strep or pPlxdc2-FcS. The protein-containing cell culture supernatant was
572 filtered through 0.22µm PES membranes (Millipore) and passed over 0.5ml of a Strep-Tactin Superflow (IBA
573 Lifesciences) matrix in a gravity flow Omniprep column (BioRad). Bound protein was washed with approximately
574 50ml phosphate buffered saline pH 7.4 (PBS) and eluted in 1ml fractions with 3mM desthiobiotin (Sigma-Aldrich)
575 in PBS. Recombinant Plxcd1 ectodomain or Plxdc2 ectodomain protein was purified under native conditions by
576 Ni-NTA chromatography from 293T cell culture supernatant. 293T cells were transfected pcDNA6-ectoPlxdc1-
577 6XHis or pcDNA6-ectoPlxdc2-6XHis using PEI transfectio. The protein-containing cell culture supernatant was
578 filtered through 0.22µm PES membranes (Millipore), concentrated using VIVAFLOW 50R (Sartorius) and passed
579 over 1ml of a Ni-NTA Agarose (Macherey-Nagel) matrix in a gravity flow Omniprep column (BioRad). Bound
580 protein was washed with approximately 50ml TBS (150 mM NaCl, 50 mM Tris-HCl, pH 7.6) and eluted in 1ml
581 fractions with 500 mM Imidazole in TBS. Protein-containing fractions were pooled, concentrated via VivaSpin
582 columns (Sartorius) and applied over Äkta Avant (GE) on a HiPrep 16/60 Sephacryl S300HR column (GE). For all
583 recombinant proteins,protein-containing fractions were pooled and buffer exchange to PBS via VivaSpin columns

584 (Sartorius) was performed. Protein concentration was determined by absorbance at 280nm. Aliquots were frozen
585 and stored at −80°C. Recombinant, human, soluble EphB3-Fc (5667-B3-050) was purchased from R&D Systems.

586 **Lentivirus production and transduction**. For production of lentiviral particles, 10cm cell culture grade petri
587 dishes of approximately 80% confluent 293T cells were transfected with 1.4µg pMD2.G (VSV-G envelope
588 expressing plasmid, a gift from Didier Trono (Addgene plasmid #12259), 3.6µg psPAX2 (Gag-Pol expression
589 construct, a gift from Didier Trono (Addgene plasmid #12260), and 5µg of lentiviral expression constructs (pLenti
590 CMV Blast DEST (706-1), pLenti-CMV-Blast-EphA7-Strep, pLenti-CMV-Blast-Plxdc1-Strep, pLenti-CMV-Blast-
591 Plxdc2-Strep) using PEI as described before (20). The supernatant containing the pseudotyped lentiviral particles
592 was harvested 2 to 3 days after transfection and filtered through 0.45µm CA membranes (Millipore). For
593 transduction, lentivirus stocks were used at a 1:5 dilution unless stated otherwise. After 48h, the selection
594 antibiotic blasticidin (Invivogen) was added to a final concentration of 10µg/ml. After initial selection the
595 blasticidin concentration was reduced to 5µg/ml.

596 **Quantitative realtime-PCR-based viral genome copy number analysis and virus attachment assay.**
597 Concentrated virus samples were treated with DNAseI (0.1 units/µl) to remove any non-encapsidated DNA (37°C,
598 overnight). Subsequently, DNAseI was deactivated and viral capsids were disrupted by heating the samples to
599 95°C for 30 minutes. Realtime-PCR (qPCR) was performed on a StepOne Plus cycler (Thermo Fisher Scientific) in
600 20µl reactions using the SensiFAST Probe Hi-ROX Kit (Bioline) (cycling conditions: 3min initial denaturation at
601 95°C, 40 cycles 95°C for 10s and 60°C for 35s). All primer-probe sets were purchased from IDT as complete
602 PrimeTime qPCR Assays (primer:probe ratio = 4:1). Samples were analyzed in technical triplicates. A series of five
603 10-fold dilutions of bacmid DNA was used as standard for absolute quantification of viral genome copies based
604 on qPCR of ORF73 for RRV (see S1 Table for a complete list of primers). For virus attachment assays transduced
605 Raji cells were incubated with ice-cold virus dilutions at the indicated concentrations, normalized to genomes
606 per cell, at 4°C for 30min. After three washes with ice-cold PBS genomic DNA was isolated using the ISOLATE II
607 Genomic DNA Kit (Bioline) according to manufacturer's instructions. Genome copies of used input virus
608 preparations were determined after overnight DNAseI digest as described above. Relative values of bound viral
609 genomes to cellular DNA were calculated on the basis of ΔCt values for viral genomic loci (ORF73 for RRV) and a
610 cellular genomic locus (CCR5) using the same conditions described above. For attachment assays all samples
611 were analyzed in technical duplicates.

612 **Infection assays, blocking experiments and flow cytometry.** For infection assays cells were plated at 50 000
613 cells/cm^2 (SLK, HaCaT, Raji), 25 000 cells/cm^2 (RF) or 200 000 cells/ml (Raji, MFB5487, MMB1845) respectively.
614 One day after plating (for adherent cells lines) or directly after plating (for suspension cell lines), cells were
615 infected with the indicated amounts of virus. Adherent cells lines were harvested 24h post infection by brief
616 trypsinization, followed by addition of 5% FCS in PBS to inhibit trypsin activity. Suspension cell lines were
617 harvested 48h post infection (24h post infection for transduced Raji cells) by pipetting. Subsequently, cells were
618 pelleted by centrifugation (1200rpm, 10min), washed once with PBS, re-pelleted and fixed in PBS supplemented
619 with 4% formaldehyde (Carl Roth). Block of RRV infection with soluble decoy receptor was assayed by infection
620 with virus inocula that were pre-incubated with the indicated concentrations of soluble EphB3-Fc, hPlxdc1-Fc,
621 hPlxdc2-Fc or Fc alone at room temperature for 30min. Calculation of molarity was based on diametric proteins.
622 Cell harvest and preparation for flow cytometry analyses was performed as described above. A minimum of 5
623 000 – 10 000 cells was analyzed per sample for YFP expression on a LSRII flow cytometer (BD Biosciences). Data
624 was analyzed using Flowing Software (Version 2.5).

625 **Immunoprecipitation and Western blot analysis.** For interaction analysis of gH-V5/gL-Flag complexes with
626 Plxdc1/2, 293T cells were transfected using PEI as described before. Lysates of 293T cells transfected with the
627 respective expression constructs for recombination gH-V5/gL-Flag complexes were prepared in NP40 lysis buffer
628 (1% Nonidet P40 Substitute (Sigma-Aldrich), 150mM NaCl (Sigma-Aldrich), 50mM HEPES (VWR), 1mM EDTA
629 (Amresco) with freshly added Protease Inhibitor Cocktail, General Use (Amresco)) and protein content was
630 determined by Bradford assay using Roti-Quant (Roth) according to manufacturer's instructions. 20µg total
631 protein was denatured in 1x SDS sample buffer (Morris formulation) at 95°C for 5min, separated by
632 polyacrylamide gel electrophoresis (PAGE) using 8–16% Tris-Glycine polyacrylamide gradient gels (Thermo Fisher
633 Scientific) with Tris-Glycine SDS running buffer (25mM Tris, 192mM glycine, 0.1% SDS) and transferred to 0.45µm
634 (0.22µm for blots containing gL) Polyvinylidendifluorid (PVDF) membranes (200mA/Gel, max 30V, 1h in Towbin
635 buffer (25mM Tris, 192mM glycine) with 20% methanol) in a wet tank system (Mini Blot Module, Thermo Fisher).
636 The membranes were blocked in 5% dry milk powder in TBS-T (5mM Tris, 15mM NaCl, 0.05% Tween20) for 1h,
637 at room temperature, washed once in TBS-T and incubated with the respective antibodies for 2h at room
638 temperature or overnight at 4°C (see S1 Table for a complete list of antibodies). After three washes with TBS-T,
639 the membranes were incubated with the respective HRP-conjugated secondary antibody in 5% dry milk powder
640 in TBS-T for 1h at room temperature washed three times in TBS-T and imaged on an ECL ChemoCam 3.2 Imager

641 (Intas) using Immobilon Forte Western HRP substrate (Merck Millipore). For pulldown of gH-V5 or gH-V5/ gL-Flag
642 complexes, the amount of input lysate between wt and mutant gH constructs was normalized to gH expression
643 as determined by Western blot and diluted to equal volume with cell lysate from non-transfected 293T cells prior
644 to immunoprecipitation. Subsequently, lysates were incubated with 0.5µg V5-tag antibody (Bio-Rad) and
645 ProteinG sepharose (GenScript) overnight at 4°C with agitation. After three washes in NP40 lysis buffer, ProteinG
646 beads with pre-coupled complexes were incubated overnight at 4°C with agitation with lysate of full-length
647 human or macaca mulatta Plxdc1-myc or Plxdc2-myc expression plasmid transfected 293T cells normalized to
648 Plxdc expression. Volumes were adjusted with lysate from untransfected 293T cells. ProteinG beads were
649 collected by brief centrifugation and washed 3 times in NP40 lysis buffer. Precipitates were heated in 2x SDS
650 sample buffer (95°C, 5min) and analyzed by Western blot as described above. For co-immunoprecipitation of
651 soluble Plxdc1/2-Strep constructs with gH-V5/gL-Flag and EphB3-myc, supernatant of Plxdc1/2-FcStrep
652 transfected 293T cells was incubated with StrepTactinXT beads (IBA) overnight at 4°C with agitation. After three
653 washes in NP40 lysis buffer, StrepTactinXT beads with pre-coupled Plxdc1/2-Strep were incubated overnight at
654 4°C with agitation with equal amounts of lysate of full-length human EphB3-myc, RRV 26-95 gH-V5/gL-Flag or
655 17577 gH-V5/gL-Flag expression plasmid transfected 293T cells or the indicated combinations. Volumes were
656 adjusted with lysate of untransfected 293T cells.

657 **Enzyme-linked immunosorbent assay (ELISA).** F96 Maxisorp Nunc-Immuno Plates (Thermo Fisher Scientific)
658 were coated with recombinant RRV 26-95 gH-FcStrep/gL (described previously (14)) at 1µg/ml in PBS overnight.
659 After three washes with PBS-T, the wells were blocked with 10% FBS in PBS for 2h. Incubation with Plxdc1
660 ectodomain or Plxdc2 ectodomain was performed for 2h at room temperature in 10% FBS in PBS. The plates
661 were washed three times with PBS-T. Bound protein was detected via the C-terminal 6XHis Tag using 6XHis
662 Antibody MA1-135 (Invitrogen) followed by three washes in TBS-T and incubation with donkey anti-mouse
663 horseradish peroxidase (HRP)-coupled secondary antibody (Dianova). After three washes, 3,3',5,5'-
664 Tetramethylbenzidin (TMB) substrate (Thermo Fisher Scientific) was added and the reaction was stopped by
665 adding 1M HCl. The plates were imaged on a Biotek Synergy 2 plate reader.

666
667 **Structure prediction and analysis.** Homology based structure prediction was performed using the Iterative
668 Threading ASSembly Refinement (I-TASSER) server on standard settings for structure prediction of RRV 26-95 gH
669 and gL based on the crystal structure of the EBV gH/gL complex (3PHF). Modeling of the RRV 26-95 gH/gL complex

670 was additionally performed using both the SPRING and CO-THreader algorithms for protein-protein complex
671 structure and multi-chain protein threading with no differences between determined structures. Resulting I-
672 TASSER structures were aligned to the gH/gL CO-THreader model with the VMD 1.9.3 OpenGL RMSD Trajectory
673 Tool based on amino acids 25 to 62 of gH (RMSD of 0.344Å) and amino acids 2 to 100 of gL (RMSD of 2.697Å) to
674 generate the depicted model. All further analyses and visualizations were performed using VMD 1.9.3 OpenGL.

675 **Mathematical and statistical analysis**. Statistical difference between groups was determined by unpaired
676 Student's t-tests followed by Bonferroni correction for multiple comparisons. All Statistical analyses were
677 performed with GraphPad Prism version 6. For all statistics, *: p-value < 0.05, **: p-value < 0.01, ***: p-value <
678 0.001, ns: not significant.

679 **ACKNOWLEDGMENTS**

680 This work was supported by grants to A.S.H. from the Deutsche Forschungsgemeinschaft (HA 6013/1,
681 HA 6013/4-1), the Wilhelm-Sander Foundation (project 2019.027.1), and the Interdisciplinary Center
682 for Clinical Research Erlangen (IZKF, grant J44), by the Deutsche Forschungsgemeinschaft, grants CRC
683 796, TP B1 to A.E., by grant RO1 AI072004 from the National Institutes of Health (NIH) to R.C.D., and
684 by base grant RR00168 from the NIH to the New England Primate Research Center.

685 **LITERATURE**

686 1. Desrosiers RC, Sasseville VG, Czajak SC, Zhang X, Mansfield KG, Kaur A, Johnson RP, Lackner
687 AA, Jung JU. 1997. A herpesvirus of rhesus monkeys related to the human Kaposi's sarcoma-
688 associated herpesvirus. J Virol 71:9764–9769.

689 2. Searles RP, Bergquam EP, Axthelm MK, Wong SW. 1999. Sequence and genomic analysis of a
690 Rhesus macaque rhadinovirus with similarity to Kaposi's sarcoma-associated herpesvirus/human
691 herpesvirus 8. J Virol 73:3040–3053.

692 3. O'Connor CM, Kedes DH. 2007. Rhesus Monkey Rhadinovirus: A Model for the Study of KSHV,
693 p. 43–69. *In* Boshoff, C, Weiss, RA (eds.), Kaposi Sarcoma Herpesvirus: New Perspectives. Springer
694 Berlin Heidelberg.

695 4. Shin YC, Jones LR, Manrique J, Lauer W, Carville A, Mansfield KG, Desrosiers RC. 2010.
696 Glycoprotein gene sequence variation in rhesus monkey rhadinovirus. Virology 400:175–186.

697 5. Bilello JP, Morgan JS, Damania B, Lang SM, Desrosiers RC. 2006. A Genetic System for Rhesus
698 Monkey Rhadinovirus: Use of Recombinant Virus To Quantitate Antibody-Mediated Neutralization. J
699 Virol 80:1549–1562.

700 6. Estep RD, Powers MF, Yen BK, Li H, Wong SW. 2007. Construction of an Infectious Rhesus
701 Rhadinovirus Bacterial Artificial Chromosome for the Analysis of Kaposi's Sarcoma-Associated
702 Herpesvirus-Related Disease Development. J Virol 81:2957–2969.

703 7. Bilello JP, Lang SM, Wang F, Aster JC, Desrosiers RC. 2006. Infection and Persistence of
704 Rhesus Monkey Rhadinovirus in Immortalized B-Cell Lines. J Virol 80:3644–3649.

705 8. Wong SW, Bergquam EP, Swanson RM, Lee FW, Shiigi SM, Avery NA, Fanton JW, Axthelm MK.
706 1999. Induction of B cell hyperplasia in simian immunodeficiency virus-infected rhesus macaques
707 with the simian homologue of Kaposi's sarcoma-associated herpesvirus. J Exp Med 190:827–840.

708 9. Orzechowska BU, Powers MF, Sprague J, Li H, Yen B, Searles RP, Axthelm MK, Wong SW.
709 2008. Rhesus macaque rhadinovirus-associated non-Hodgkin lymphoma: animal model for KSHV-
710 associated malignancies. Blood 112:4227–4234.

711 10. Bruce AG, Bielefeldt-Ohmann H, Barcy S, Bakke AM, Lewis P, Tsai C-C, Murnane RD, Rose TM.
712 2012. Macaque Homologs of EBV and KSHV Show Uniquely Different Associations with Simian AIDS-
713 related Lymphomas. PLoS Pathog 8:e1002962.

714 11. Marshall VA, Labo N, Hao X-P, Holdridge B, Thompson M, Miley W, Brands C, Coalter V, Kiser
715 R, Anver M, Golubeva Y, Warner A, Jaffe ES, Piatak M, Wong SW, Ohlen C, MacAllister R, Smedley J,
716 Deleage C, Del Prete GQ, Lifson JD, Estes JD, Whitby D. 2018. Gammaherpesvirus infection and
717 malignant disease in rhesus macaques experimentally infected with SIV or SHIV. PLOS Pathog
718 14:e1007130.

719 12. Umbach JL, Strelow LI, Wong SW, Cullen BR. 2010. Analysis of rhesus rhadinovirus microRNAs
720 expressed in virus-induced tumors from infected rhesus macaques. Virology 405:592–599.

721 13. Ensser A, Yasuda K, Lauer W, Desrosiers RC, Hahn AS. 2020. Rhesus Monkey Rhadinovirus
722 Isolated from Hemangioma Tissue. Microbiol Resour Announc 9.

723 14. Hahn AS, Kaufmann JK, Wies E, Naschberger E, Panteleev-Ivlev J, Schmidt K, Holzer A,
724 Schmidt M, Chen J, König S, Ensser A, Myoung J, Brockmeyer NH, Stürzl M, Fleckenstein B, Neipel F.
725 2012. The ephrin receptor tyrosine kinase A2 is a cellular receptor for Kaposi's sarcoma–associated
726 herpesvirus. Nat Med 18:961–966.

727 15. Hahn AS, Desrosiers RC. 2013. Rhesus Monkey Rhadinovirus Uses Eph Family Receptors for
728 Entry into B Cells and Endothelial Cells but Not Fibroblasts. PLoS Pathog 9:e1003360.

729 16. TerBush AA, Hafkamp F, Lee HJ, Coscoy L. 2018. A Kaposi's Sarcoma-Associated Herpesvirus
730 Infection Mechanism Is Independent of Integrins α3β1, αVβ3, and αVβ5. J Virol 92:e00803-18,
731 /jvi/92/17/e00803-18.atom.

732 17. Chen J, Zhang X, Schaller S, Jardetzky TS, Longnecker R. 2019. Ephrin Receptor A4 is a New
733 Kaposi's Sarcoma-Associated Herpesvirus Virus Entry Receptor. mBio 10:e02892-18,
734 /mbio/10/1/mBio.02892-18.atom.

735 18. Hahn AS, Desrosiers RC. 2014. Binding of the Kaposi's sarcoma-associated herpesvirus to the
736 ephrin binding surface of the EphA2 receptor and its inhibition by a small molecule. J Virol 88:8724–
737 8734.

738 19. Kumar B, Chandran B. 2016. KSHV Entry and Trafficking in Target Cells-Hijacking of Cell Signal
739 Pathways, Actin and Membrane Dynamics. Viruses 8.

740 20. Großkopf AK, Schlagowski S, Hörnich BF, Fricke T, Desrosiers RC, Hahn AS. 2019. EphA7
741 Functions as Receptor on BJAB Cells for Cell-to-Cell Transmission of the Kaposi's Sarcoma-Associated
742 Herpesvirus and for Cell-Free Infection by the Related Rhesus Monkey Rhadinovirus. J Virol

743 93:e00064-19, /jvi/93/15/JVI.00064-19.atom.

744 21. Möhl BS, Chen J, Longnecker R. 2019. Gammaherpesvirus entry and fusion: A tale how two
745 human pathogenic viruses enter their host cells, p. 313–343. *In* Advances in Virus Research. Elsevier.

746 22. TerBush AA, Hafkamp F, Lee HJ, Coscoy L. 2018. A Kaposi's Sarcoma-Associated Herpesvirus
747 Infection Mechanism is Independent of Integrins α3β1, αVβ3, and αVβ5. J Virol
748 https://doi.org/10.1128/JVI.00803-18.

749 23. Großkopf AK, Ensser A, Neipel F, Jungnickl D, Schlagowski S, Desrosiers RC, Hahn AS. 2018. A
750 conserved Eph family receptor-binding motif on the gH/gL complex of Kaposi's sarcoma-associated
751 herpesvirus and rhesus monkey rhadinovirus. PLOS Pathog 14:e1006912.

752 24. Hahn AS, Bischof GF, Großkopf AK, Shin YC, Domingues A, Gonzalez-Nieto L, Rakasz EG,
753 Watkins DI, Ensser A, Martins MA, Desrosiers RC. 2019. A Recombinant Rhesus Monkey Rhadinovirus
754 Deleted of Glycoprotein L Establishes Persistent Infection of Rhesus Macaques and Elicits
755 Conventional T Cell Responses. J Virol JVI.01093-19, jvi;JVI.01093-19v1.

756 25. Croix BSt. 2000. Genes Expressed in Human Tumor Endothelium. Science 289:1197–1202.

757 26. Carson-Walter EB, Watkins DN, Nanda A, Vogelstein B, Kinzler KW, St Croix B. 2001. Cell
758 surface tumor endothelial markers are conserved in mice and humans. Cancer Res 61:6649–6655.

759 27. Miller-Delaney SFC, Lieberam I, Murphy P, Mitchell KJ. 2011. Plxdc2 is a mitogen for neural
760 progenitors. PloS One 6:e14565.

761 28. Lee HK, Bae HR, Park HK, Seo IA, Lee EY, Suh DJ, Park HT. 2005. Cloning, characterization and
762 neuronal expression profiles of tumor endothelial marker 7 in the rat brain. Brain Res Mol Brain Res
763 136:189–198.

764 29. Miller SFC, Summerhurst K, Rünker AE, Kerjan G, Friedel RH, Chédotal A, Murphy P, Mitchell
765 KJ. 2007. Expression of Plxdc2/TEM7R in the developing nervous system of the mouse. Gene Expr
766 Patterns GEP 7:635–644.

767 30. Nanda A, Buckhaults P, Seaman S, Agrawal N, Boutin P, Shankara S, Nacht M, Teicher B,
768 Stampfl J, Singh S, Vogelstein B, Kinzler KW, St. Croix B. 2004. Identification of a Binding Partner for
769 the Endothelial Cell Surface Proteins TEM7 and TEM7R. Cancer Res 64:8507–8511.

770 31. Cheng G, Zhong M, Kawaguchi R, Kassai M, Al-Ubaidi M, Deng J, Ter-Stepanian M, Sun H.
771 2014. Identification of PLXDC1 and PLXDC2 as the transmembrane receptors for the multifunctional
772 factor PEDF. eLife 3:e05401.

773 32. Lee HK, Seo IA, Park HK, Park HT. 2006. Identification of the basement membrane protein
774 nidogen as a candidate ligand for tumor endothelial marker 7 in vitro and in vivo. FEBS Lett
775 580:2253–2257.

776 33. Uhlen M, Fagerberg L, Hallstrom BM, Lindskog C, Oksvold P, Mardinoglu A, Sivertsson A,
777 Kampf C, Sjostedt E, Asplund A, Olsson I, Edlund K, Lundberg E, Navani S, Szigyarto CA-K, Odeberg J,
778 Djureinovic D, Takanen JO, Hober S, Alm T, Edqvist P-H, Berling H, Tegel H, Mulder J, Rockberg J,
779 Nilsson P, Schwenk JM, Hamsten M, von Feilitzen K, Forsberg M, Persson L, Johansson F, Zwahlen M,
780 von Heijne G, Nielsen J, Ponten F. 2015. Tissue-based map of the human proteome. Science
781 347:1260419–1260419.

782 34. Matsuura H, Kirschner AN, Longnecker R, Jardetzky TS. 2010. Crystal structure of the Epstein-
783 Barr virus (EBV) glycoprotein H/glycoprotein L (gH/gL) complex. Proc Natl Acad Sci 107:22641–22646.

784 35. Tischer BK, Smith GA, Osterrieder N. 2010. En Passant Mutagenesis: A Two Step Markerless
785 Red Recombination System, p. 421–430. *In* Braman, J (ed.), In Vitro Mutagenesis Protocols. Humana
786 Press, Totowa, NJ.

787 36. Li Q, Turk SM, Hutt-Fletcher LM. 1995. The Epstein-Barr virus (EBV) BZLF2 gene product
788 associates with the gH and gL homologs of EBV and carries an epitope critical to infection of B cells
789 but not of epithelial cells. J Virol 69:3987–3994.

790 37. Nguyen C, Kamil J. 2018. Pathogen at the Gates: Human Cytomegalovirus Entry and Cell

791 Tropism. Viruses 10:704.

792 38. Wang X, Kenyon WJ, Li Q, Müllberg J, Hutt-Fletcher LM. 1998. Epstein-Barr Virus Uses
793 Different Complexes of Glycoproteins gH and gL To Infect B Lymphocytes and Epithelial Cells. J Virol
794 72:5552–5558.

795 39. Chen J, Sathiyamoorthy K, Zhang X, Schaller S, Perez White BE, Jardetzky TS, Longnecker R.
796 2018. Ephrin receptor A2 is a functional entry receptor for Epstein-Barr virus. Nat Microbiol
797 https://doi.org/10.1038/s41564-017-0081-7.

798 40. Hirai H, Maru Y, Hagiwara K, Nishida J, Takaku F. 1987. A novel putative tyrosine kinase
799 receptor encoded by the eph gene. Science 238:1717–1720.

800 41. Pasquale EB. 2010. Eph receptors and ephrins in cancer: bidirectional signalling and beyond.
801 Nat Rev Cancer 10:165–180.

802 42. Zhang Z-Z, Hua R, Zhang J-F, Zhao W-Y, Zhao E-H, Tu L, Wang C-J, Cao H, Zhang Z-G. 2015.
803 TEM7 (PLXDC1), a key prognostic predictor for resectable gastric cancer, promotes cancer cell
804 migration and invasion. Am J Cancer Res 5:772–781.

805 43. Carpenter RL, Paw I, Zhu H, Sirkisoon S, Xing F, Watabe K, Debinski W, Lo H-W. 2015. The
806 gain-of-function GLI1 transcription factor TGLI1 enhances expression of VEGF-C and TEM7 to
807 promote glioblastoma angiogenesis. Oncotarget 6:22653–22665.

808 44. Czekierdowski A, Stachowicz N, Czekierdowska S, Łoziński T, Gurynowicz G, Kluz T. 2018.
809 Prognostic significance of TEM7 and nestin expression in women with advanced high grade serous
810 ovarian cancer. Ginekol Pol 89:135–141.

811 45. Kim GH, Won JE, Byeon Y, Kim MG, Wi TI, Lee JM, Park Y-Y, Lee J-W, Kang TH, Jung ID, Shin
812 BC, Ahn HJ, Lee YJ, Sood AK, Han HD, Park Y-M. 2018. Selective delivery of PLXDC1 small interfering
813 RNA to endothelial cells for anti-angiogenesis tumor therapy using CD44-targeted chitosan
814 nanoparticles for epithelial ovarian cancer. Drug Deliv 25:1394–1402.

815 46. Falchetti ML, D'Alessandris QG, Pacioni S, Buccarelli M, Morgante L, Giannetti S, Lulli V,
816 Martini M, Larocca LM, Vakana E, Stancato L, Ricci-Vitiani L, Pallini R. 2019. Glioblastoma
817 endothelium drives bevacizumab-induced infiltrative growth via modulation of PLXDC1. Int J Cancer
818 144:1331–1344.

819 47. Hahn AS, Großkopf AK, Jungnickl D, Scholz B, Ensser A. 2016. Viral FGARAT Homolog ORF75
820 of Rhesus Monkey Rhadinovirus Effects Proteasomal Degradation of the ND10 Components SP100
821 and PML. J Virol 90:8013–8028.

822 48. Shin YC, Desrosiers RC. 2011. Rhesus Monkey Rhadinovirus ORF57 Induces gH and gL
823 Glycoprotein Expression through Posttranscriptional Accumulation of Target mRNAs. J Virol 85:7810–
824 7817.

825 49. Hahn A, Birkmann A, Wies E, Dorer D, Mahr K, Sturzl M, Titgemeyer F, Neipel F. 2009.
826 Kaposi's Sarcoma-Associated Herpesvirus gH/gL: Glycoprotein Export and Interaction with Cellular
827 Receptors. J Virol 83:396–407.

828 50. Longo PA, Kavran JM, Kim M-S, Leahy DJ. 2013. Transient Mammalian Cell Transfection with
829 Polyethylenimine (PEI), p. 227–240. *In* Methods in Enzymology. Elsevier.

830

831 **S1 Table. List of primers, and antibodies used in this study.**

832

833

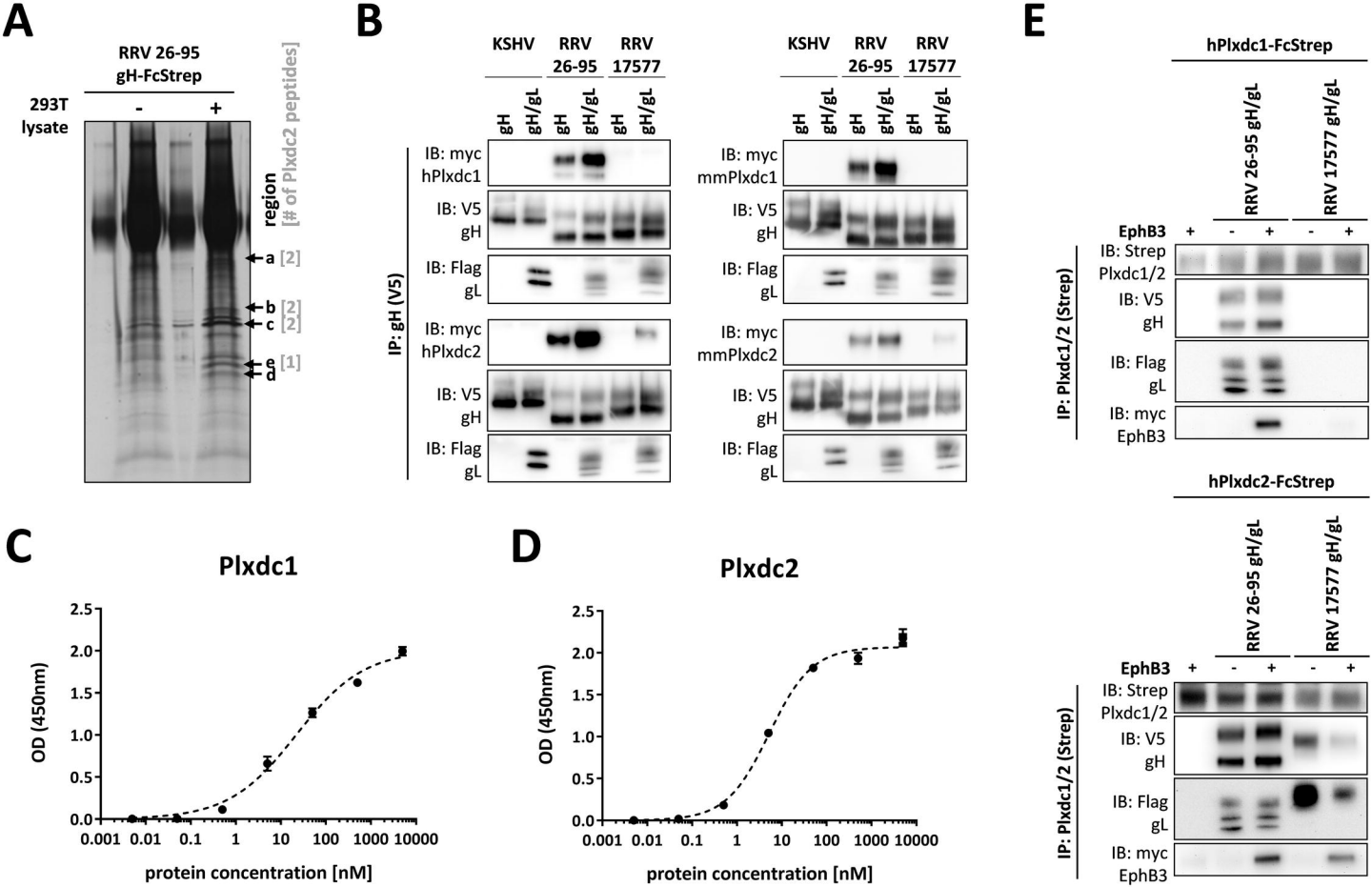
A
RRV 26-95
gH-FcStrep
293T lysate
-
+
region
[# of Plxdc2 peptides]
a [2]
b [2]
c [2]
e [1]
d
B
KSHV
RRV 26-95
RRV 17577
gH
gH/gL
IP: gH (V5)
IB: myc hPlxdc1
IB: V5 gH
IB: Flag gL
IB: myc hPlxdc2
IB: myc mmPlxdc1
IB: myc mmPlxdc2
C
Plxdc1
OD (450nm)
protein concentration [nM]
D
Plxdc2
E
hPlxdc1-FcStrep
hPlxdc2-FcStrep
RRV 26-95 gH/gL
RRV 17577 gH/gL
EphB3
IP: Plxdc1/2 (Strep)
IB: Strep Plxdc1/2
IB: V5 gH
IB: Flag gL
IB: myc EphB3

A

Name	Mutation	Eph binding
RRV-YFP wt	wt	+
RRV-YFP gH-AELAAN	gH Val51, Glu54 and Phe55 to Ala	-

B

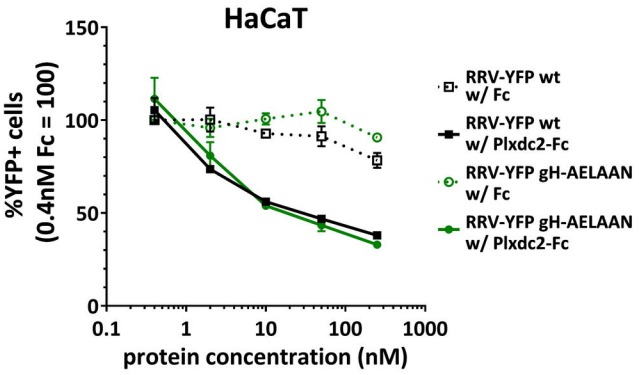

C

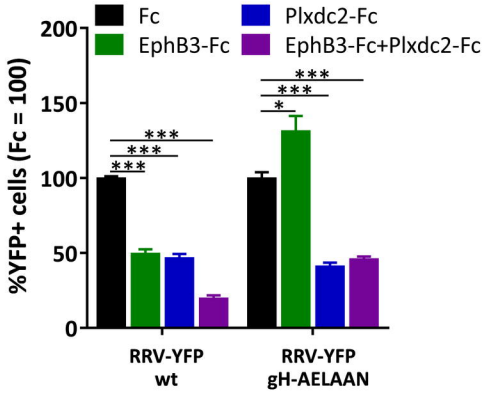

D

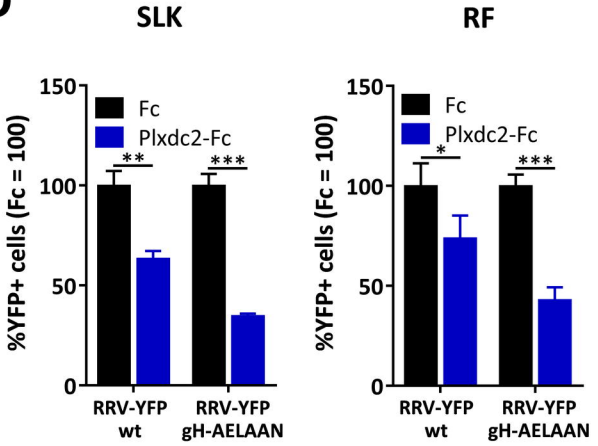

E

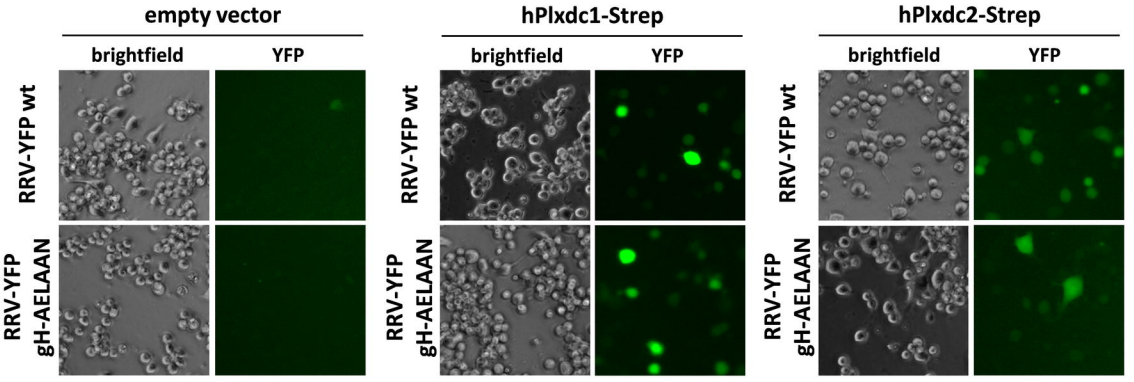

F

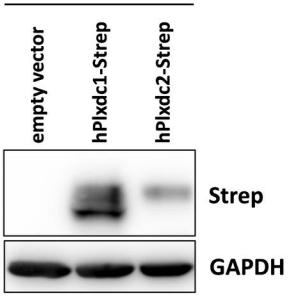

G

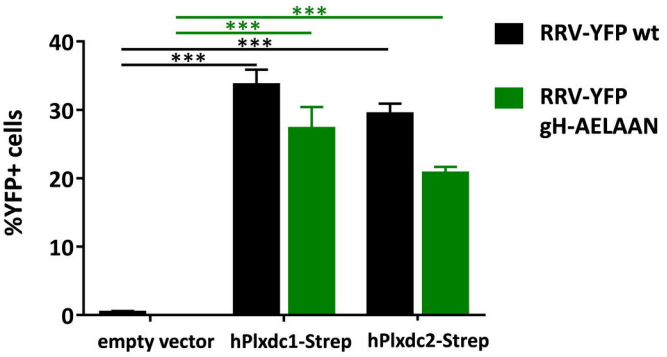

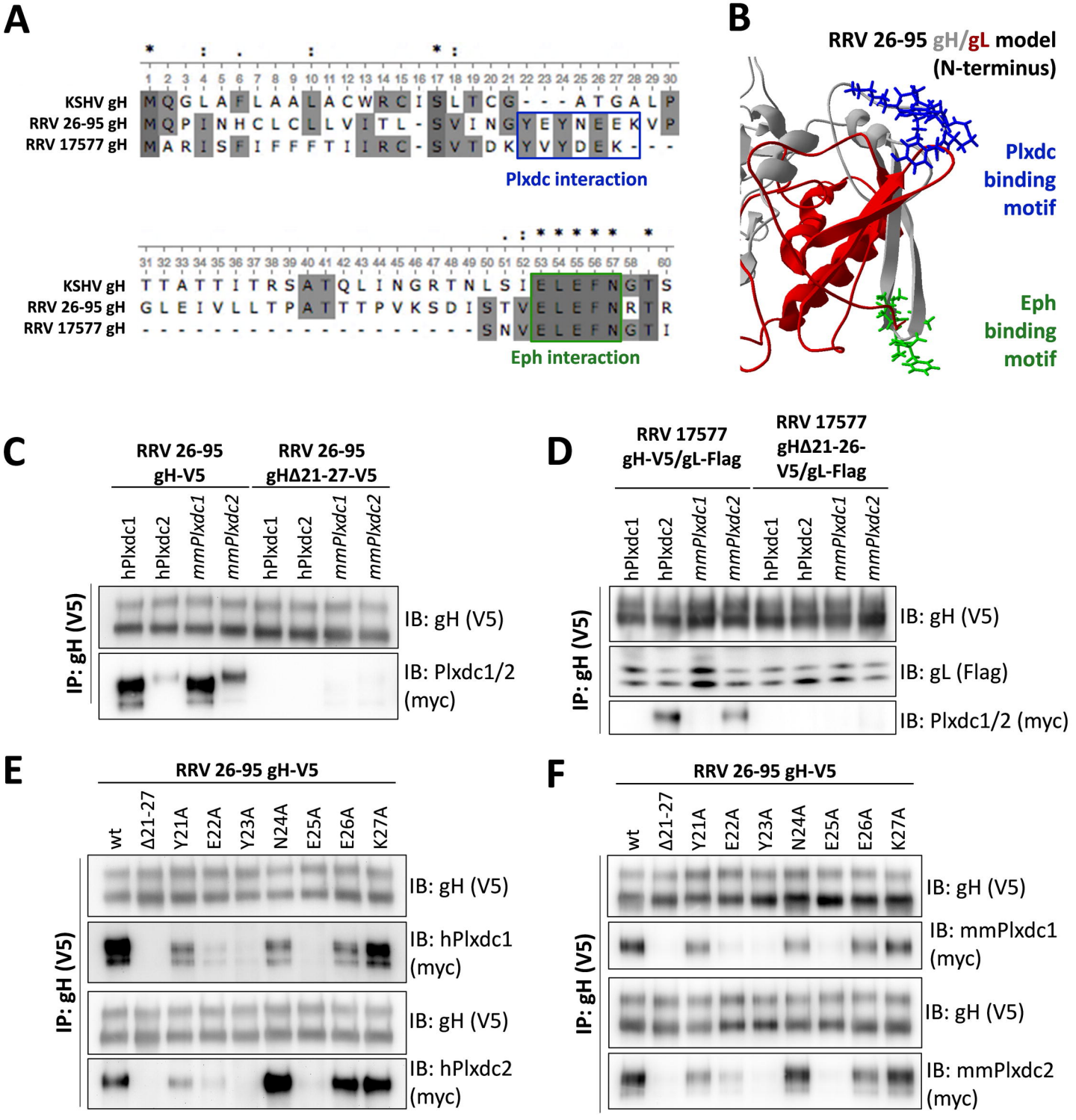
A
KSHV gH
RRV 26-95 gH
RRV 17577 gH
Plxdc interaction
Eph interaction
B
RRV 26-95 gH/gL model
(N-terminus)
Plxdc
binding
motif
Eph
binding
motif
C
RRV 26-95
gH-V5
RRV 26-95
gHΔ21-27-V5
hPlxdc1
hPlxdc2
mmPlxdc1
mmPlxdc2
IP: gH (V5)
IB: gH (V5)
IB: Plxdc1/2
(myc)
D
RRV 17577
gH-V5/gL-Flag
RRV 17577
gHΔ21-26-
V5/gL-Flag
IB: gL (Flag)
IB: Plxdc1/2 (myc)
E
RRV 26-95 gH-V5
wt
Δ21-27
Y21A
E22A
Y23A
N24A
E25A
E26A
K27A
IB: hPlxdc1
(myc)
IB: hPlxdc2
(myc)
F
IB: mmPlxdc1
(myc)
IB: mmPlxdc2
(myc)

A

Name	Mutation	Eph binding	Plxdc1/2 binding
RRV-YFP wt	wt	+	+
RRV-YFP gH-AELAAN	gH V51A-E54A-E55A	-	+
RRV-YFP gHΔ21-27	gH aa21-27 deletion	+	-
RRV-YFP gHΔ21-27-AELAAN	gH aa21-27 deletion, V51A-E54A- E55A	-	-

B

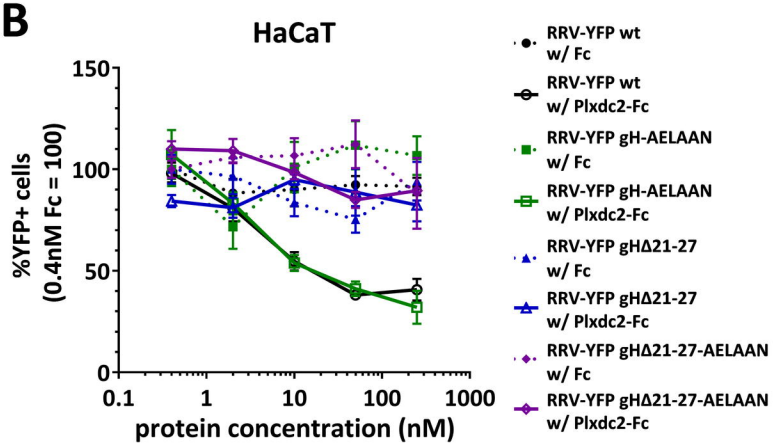

C

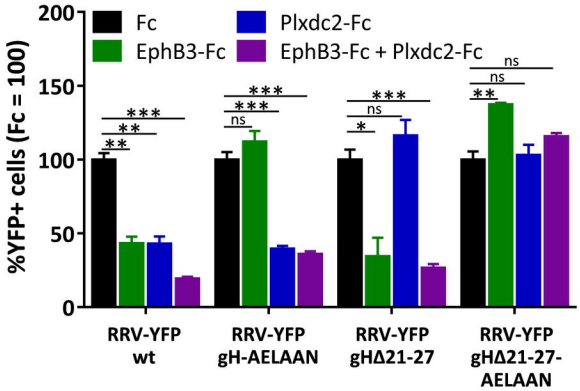

D

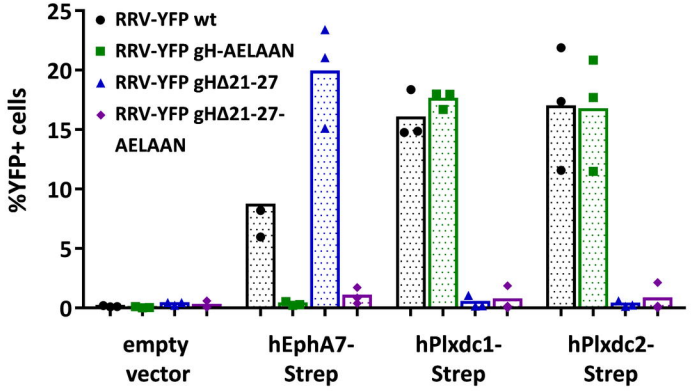

E

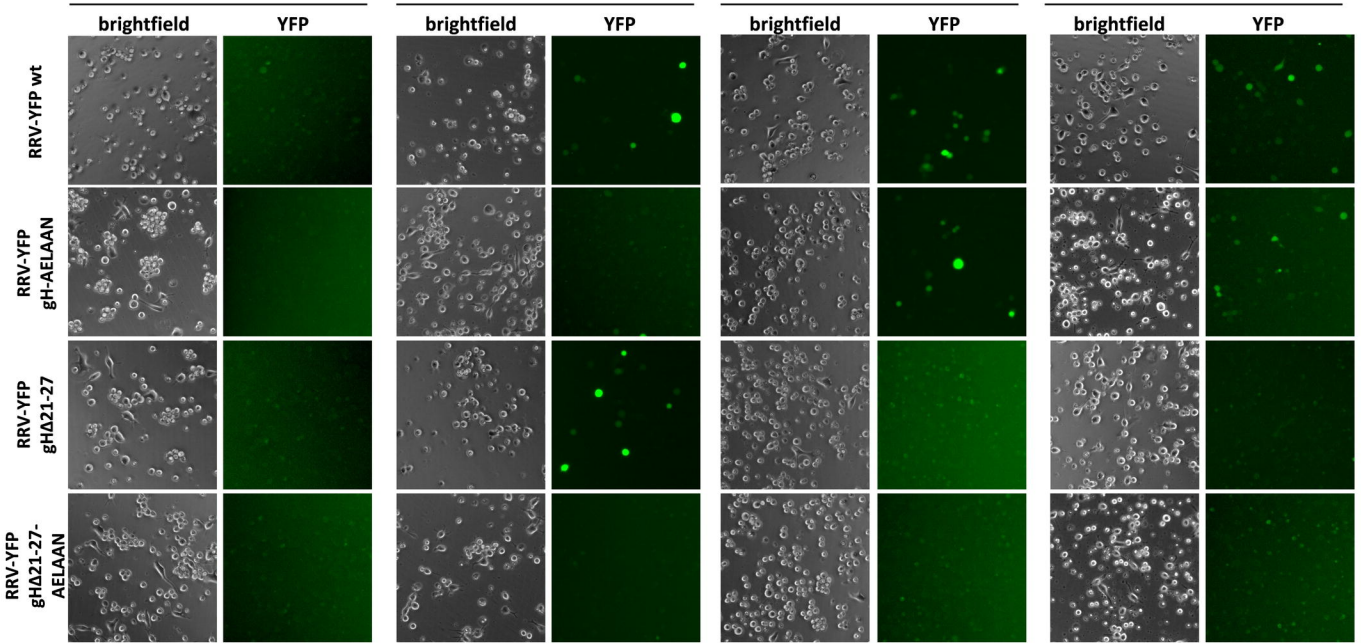

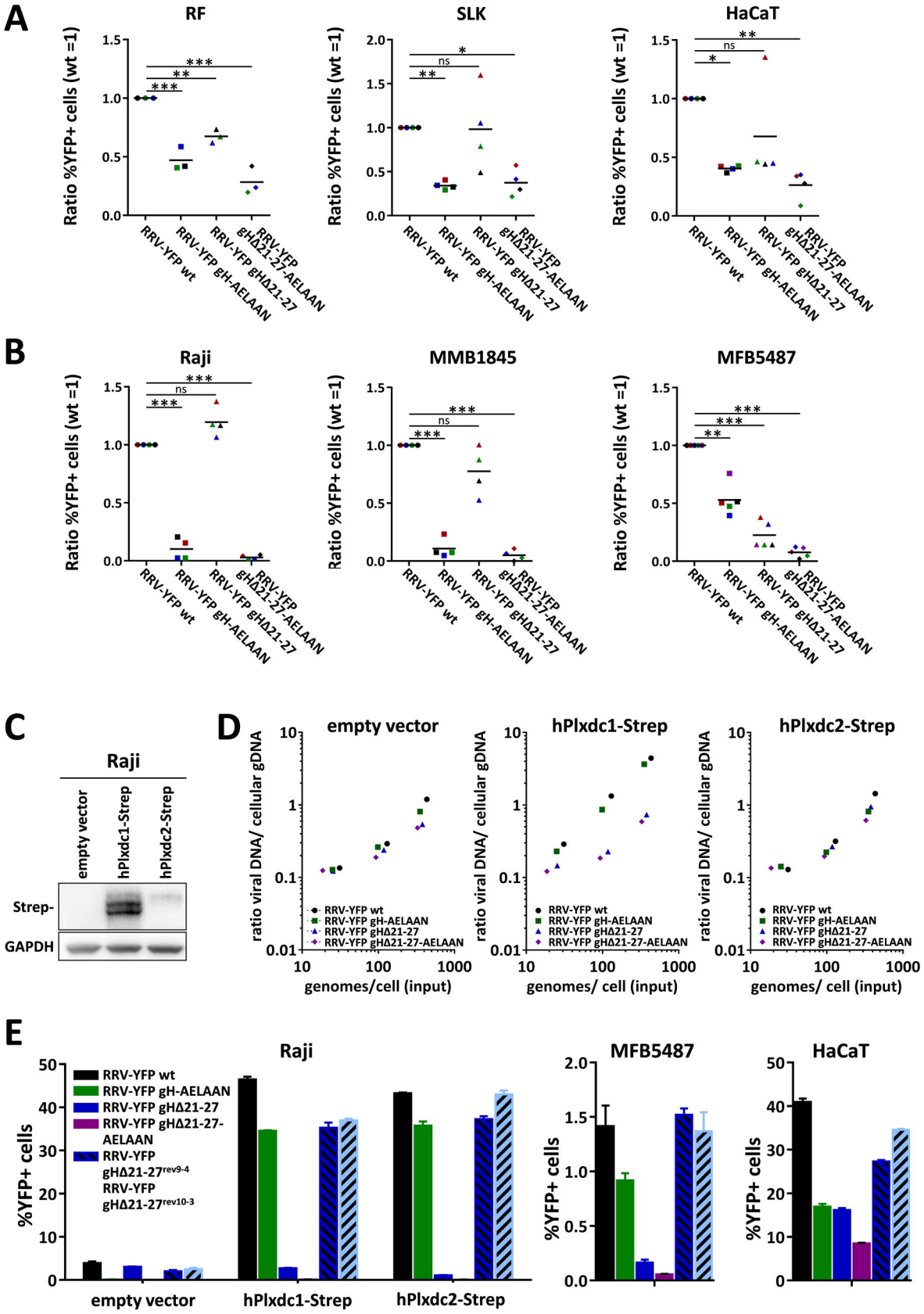
A
RF
SLK
HaCaT
Ratio %YFP+ cells (wt =1)
RRV-YFP wt
RRV-YFP gH-AELAAN
RRV-YFP gHΔ21-27
RRV-YFP gHΔ21-27-AELAAN
B
Raji
MMB1845
MFB5487
C
Raji
empty vector
hPlxdc1-Strep
hPlxdc2-Strep
Strep-
GAPDH
D
empty vector
hPlxdc1-Strep
hPlxdc2-Strep
ratio viral DNA/ cellular gDNA
genomes/cell (input)
genomes/ cell (input)
RRV-YFP wt
RRV-YFP gH-AELAAN
RRV-YFP gHΔ21-27
RRV-YFP gHΔ21-27-AELAAN
E
Raji
MFB5487
HaCaT
%YFP+ cells
RRV-YFP wt
RRV-YFP gH-AELAAN
RRV-YFP gHΔ21-27
RRV-YFP gHΔ21-27-AELAAN
RRV-YFP gHΔ21-27rev9-4
RRV-YFP gHΔ21-27rev10-3
empty vector
hPlxdc1-Strep
hPlxdc2-Strep

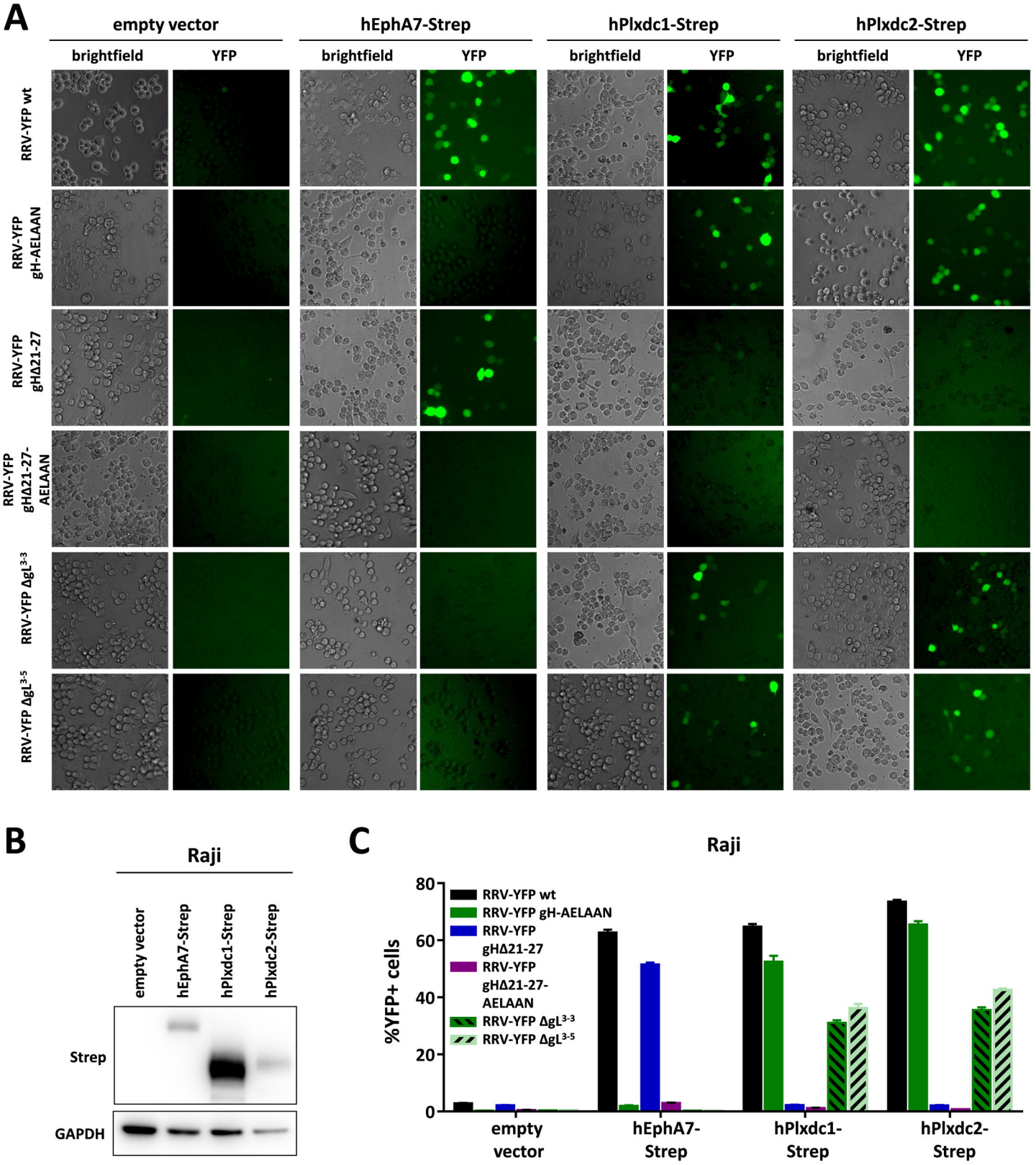
A
empty vector
hEphA7-Strep
hPlxdc1-Strep
hPlxdc2-Strep
brightfield
YFP
RRV-YFP wt
RRV-YFP gH-AELAAN
RRV-YFP gHΔ21-27
RRV-YFP gHΔ21-27-AELAAN
RRV-YFP ΔgL3-3
RRV-YFP ΔgL3-5
B
Raji
empty vector
hEphA7-Strep
hPlxdc1-Strep
hPlxdc2-Strep
Strep
GAPDH
C
Raji
%YFP+ cells
0
20
40
60
80
RRV-YFP wt
RRV-YFP gH-AELAAN
RRV-YFP gHΔ21-27
RRV-YFP gHΔ21-27-AELAAN
RRV-YFP ΔgL3-3
RRV-YFP ΔgL3-5
empty vector
hEphA7-Strep
hPlxdc1-Strep
hPlxdc2-Strep